A Journal of the Gesellschaft Deutscher Chemiker

Angewandte International Edition Chemie

GDCh

www.angewandte.org

Accepted Article

Title: Hybrid Organic-Inorganic Thermoelectric Materials and Devices

Authors: Huile Jin, Jun Li, James Iocozzia, Xin Zeng, Pai-Chun Wei, Chao Yang, Nan Li, Zhaoping Liu, Jr Hau He, Tiejun Zhu, Jichang Wang, Zhiqun Lin, and shun wang

To be cited as: *Angew. Chem. Int. Ed.* 10.1002/anie.201901106
Angew. Chem. 10.1002/ange.201901106

Link to VoR: http://dx.doi.org/10.1002/anie.201901106
http://dx.doi.org/10.1002/ange.201901106

WILEY-VCH

10.1002/anie.201901106

Hybrid Organic-Inorganic Thermoelectric Materials and Devices

Huile Jin,[+[a]] Jun Li,[+[a]] James Iocozzia,[+[b]] Xin Zeng,[+[c,d]] Pai-Chun Wei,[+[e]] Chao Yang,[[a]] Nan Li,[[d]] Zhaoping Liu,[[g]] Jr Hau He,*[[e]] Tiejun Zhu,*[[f]] Jichang Wang,*[[c]] Zhiqun Lin,*[[b]] and Shun Wang*[[a]]

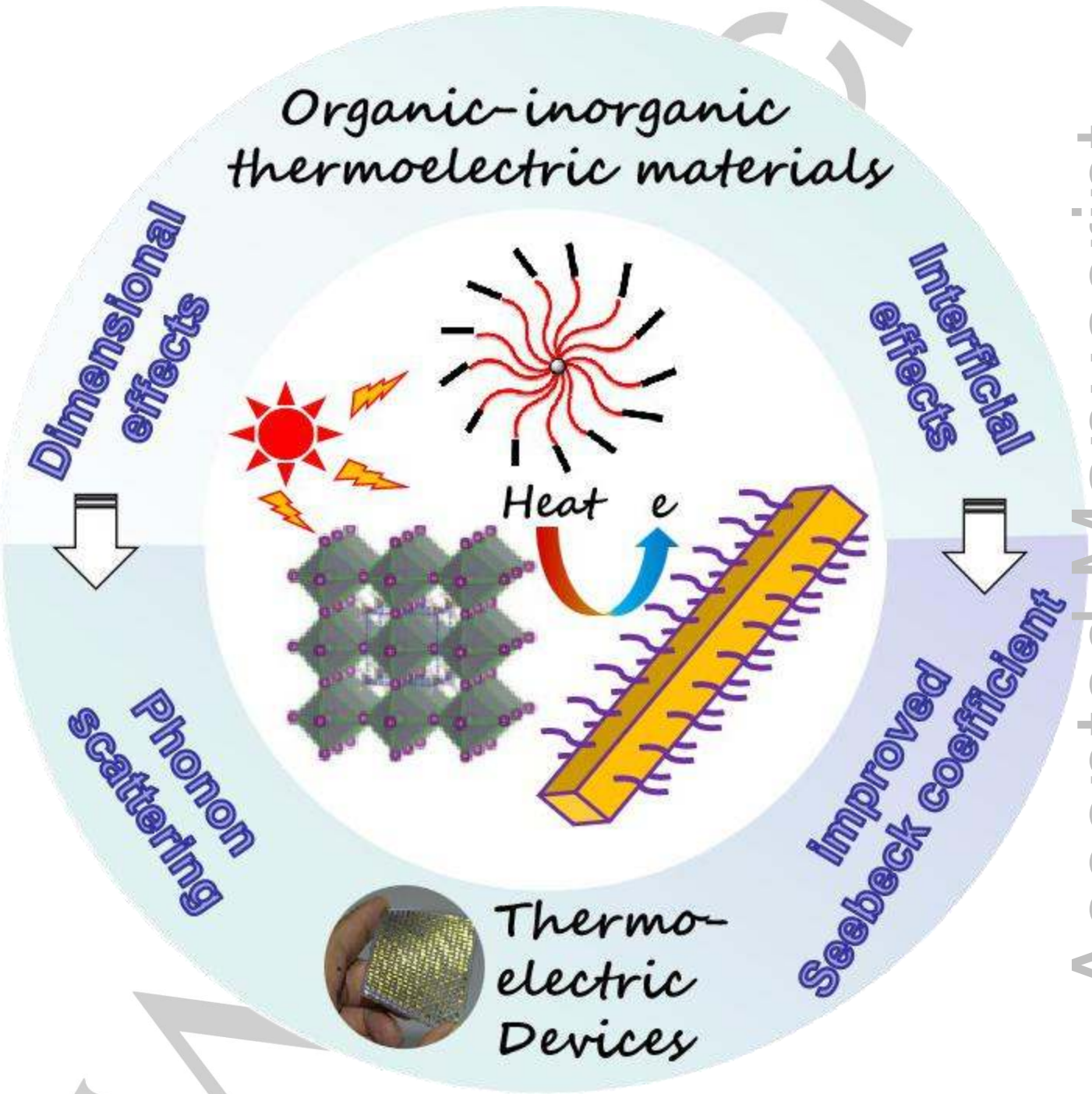

Hybrid organic-inorganic materials have been considered as a new candidate in the field of thermoelectric materials from the last decade due to their great potential to enhance the thermoelectric performance by utilizing the low thermal conductivity of organic materials and the high Seebeck coefficient, and high electrical conductivity of inorganic materials. Herein, we provide an overview of interfacial engineering in the synthesis of various organic-inorganic thermoelectric hybrid materials, along with the dimensional design for tuning their thermoelectric properties. Interfacial effects are examined in terms of nanostructures, physical properties and chemical doping between the inorganic and organic components. Several key factors which dictate the thermoelectric efficiency and performance of various electronic devices are also discussed, such as the thermal conductivity, electric transportation, electronic band structures, and band convergence of the hybrid materials.

From the Contents

1. Introduction

Thermoelectric materials enable the direct conversion between thermal and electrical energy providing an alternative mechanism for power generation. As carbon-based fossil fuels are gradually depleted, growing efforts have been invested in searching for new alternative energy resources as well as improving the efficiency of current fuel-based technologies. Considering that a large proportion of energy produced by current technologies is lost as errant heat, such as in electric power generation and transportation, thermoelectric devices can be used to directly convert this otherwise wasted thermal energy into electrical energy thus providing a promising solution for improving the fuel efficiency of established and emerging energy technologies. In comparison to other electricity generating technologies, thermoelectric devices have several attractive features including long operating lifetimes, no moving parts, no noise generation, easy maintenance, and excellent reliability.[1-5]

Thermoelectric materials, which can generate electricity from waste heat or be used as solid-state Peltier coolers, play an important role in thermoelectric devices. Most ongoing research focuses on the inorganic materials due to their high Seebeck coefficient and high electric conductivity. Typical materials being investigated include Bi_2Te_3,[6] Sb_2Te_3,[7] PbTe,[8] and other related alloys.[9] The overall thermoelectric performance is measured by a dimensionless figure of merit, $ZT = S^2\sigma T/\kappa$, where S is the Seebeck coefficient (the change in voltage per unit temperature difference in a material), σ is the electrical conductivity, κ is the thermal conductivity and T is the absolute temperature.[10] In the absence of available thermal conductivity data, the power factor $S^2\sigma$ can also be used to evaluate and compare the performance of thermoelectric materials. Unfortunately, the low efficiency and high-cost of such inorganic materials hinder their broad application. Compared to the intensive investigation on the inorganic thermoelectric materials front, less attention has been paid to organic thermoelectric materials. This likely stems from the limited range of operating temperature of such materials. Only a few organic materials are stable at elevated temperatures ranging from 500-900 K: the optimal range for massive thermoelectric energy recovery.

The figure of merit for organic thermoelectric materials is usually 2-3 orders of magnitude lower than that for inorganic thermoelectric materials due to their low electrical conductivity, Seebeck coefficient, and power factor. However, organic materials have the advantage of low density, low cost, and low thermal conductivity. Importantly, organic materials can be readily synthesized on a large scale allowing them to be used in niche applications such as room temperature cooling and power generation. For example, conductive polymers such as polypyrrole (PPy),[11] polyaniline (PANI),[12] polythiophene (PTH),[13,14] poly(3,4-ethylenedioxythiophene): poly(styrenesulfonate) (PEDOT:PSS),[15,16] and polyacetylene (PA)[17-19] have been used as thermoelectric materials owing to their low thermal conductivity. In addition these conducting polymers have the added advantage of low environmental impact.

Despite great progress achieved in previous decade, *ZT* values for current thermoelectric materials are still quite low (values less than 1). The target *ZT* value of more advanced thermoelectric materials is 3 or greater. In order to realize higher thermoelectric performance, such materials must have a high electrical conductivity, high Seebeck coefficient, and low thermal conductivity. It is especially challenging to achieve all of these requirements in one material because properties are interrelated, determined by their electronic structure (e.g., band gap, band shape, and band degeneracy near the Fermi level) and the scattering of charge carriers (electrons or holes).[20] Consequently one

[a] Prof. Dr. H. Jin, Dr. J. Li, C. Yang, Prof. Dr. S. Wang
College of Chemistry and Materials Engineering,
Institute of New Materials and Industrial Technologies,
Wenzhou University, Wenzhou, Zhejiang 325035 (China)
E-mail: shunwang@wzu.edu.cn
[b] J. Iocozzia, Prof. Dr. Z. Lin
School of Materials Science and Engineering, Georgia Institute of Technology, Atlanta GA 30332 (USA)
E-mail: zhiqun.lin@mse.gatech.edu
[c] X. Zeng, Prof. Dr. J. Wang
Department of Chemistry and Biochemistry, University of Windsor, Windsor, ON N9B 3P4 (Canada)
E-mail: jwang@uwindsor.ca
[d] X. Zeng, Prof. Dr. N. Li
College of Chemistry, Beijing Institute of Technology, Beijing 100081 (China)
[e] Pai-Chun Wei, Prof. Dr. Jr Hau He
Computer, Electrical, and Mathematical Sciences and Engineering Division, King Abdullah University of Science and Technology (KAUST), Thuwal 23955-6900 (Saudi Arabia)
[f] Prof. Dr. Tiejun Zhu
State Key Laboratory of Silicon Materials, School of Materials Science and Engineering, Zhejiang University, Hangzhou 310027 (China)
[g] Dr. Zhaoping Liu
Ningbo Institute of Materials Technology and Engineering, Chinese Academy of Sciences, Ningbo 315201 (China)
+ These authors contributed equally to this work.

Supporting information for this article is given via a link at the end of the document.

strategy to circumvent the challenge of a single thermoelectric material possessing all of the material properties is to develop hybrid thermoelectric materials combining the low thermal conductivity of organic materials and high Seeback coefficient and electric conductivity of inorganic materials. In this way, the pool of possible candidate materials is much larger and a greater emphasis is placed on constituent material synthesis, processing and combination. In this review, we highlight and summarize recent work in the development of hybrid thermoelectric materials and discuss the numerous advantages exhibited by these hybrid materials, such as the high *ZT* values, flexibility, transparency, low cost, and simplified fabrication processes. Both the synthesis routes of these new types of thermoelectric materials and the strategies of enhancing the thermoelectric performance are discussed in detail. Details of resulting devices incorporating hybrid organic-inorganic thermoelectrics are also addressed.

2. The Syntehsis of Hybrid Organic-Inorganic Thermoelectric Materials

2.1 Hybrid Polymer-Inorganic Thermoelectric Materials

Designing polymer-inorganic thermoelectric composites presents a promising approach to overcome the low electric conductivity, low Seebeck coefficient and low power factor (PF) of polymers and the high cost of inorganic reagents. Various methods have been deployed to fabricate the hybrid polymer-inorganic materials, such as physical mixing, solution mixing, and *in situ* polymerization. Notably, the thermal conductivity of polymers is about one order of magnitude lower than traditional inorganic thermoelectric materials, making polymers such as polyaniline (PANI), polythiophene (PTH), and poly(3,4-ethylenedioxythiophene) (PEDOT) great candidates in the development of new thermoelectric materials.

There are several PANI-inorganic thermoelectric nanomaterials reported in the literature in which PANI is mixed with various metal oxides such as V_2O_5,[21] $BaTiO_3$,[22] BiCuSeO,[23] $Ca_3Co_4O_9$,[24] Bi,[25,26] Bi_2Te_3 and its alloys,[27-29] $NaFe_4P_{12}$,[30] carbon nanotubes[31,32] and PbTe.[33] PANI is a typical conducting polymer with good stability and an electrical conductivity as high as 10^5 S/m. However, its power factor ($S^2\sigma$) is only on the order of 10^{-6} W/mK which is three orders of magnitude lower than that of inorganic thermoelectric materials. Despite its lower power factor, recent work on such hybrid PANI-inorganic materials has shown an improved Seebeck coefficient.[34] For example, using both the physical solid mixture and solution mixture methods Toshima et al. synthesized polyaniline (PANI)-Bi_2Te_3 nanohybrids, in which Bi_2Te_3 nanoparticles were first prepared from $BiCl_3$ and $TiCl_4$.[35] The resulting hybrid materials showed a higher thermoelectric performance than the pristine organic polymer because of an overall increase in the Seebeck coefficient despite the overall reduced electrical conductivity of the composite (see Figure 1). They have also prepared hybrid materials of PANI with Au nanoparticles (NPs) which were synthesized by successive oxidation of the residual aniline with ammonium peroxodisulfate and in situ reduction of $HAuCl_4$. The resulting hybrid nanostructures showed improved electrical conductivities as high as 330 S/cm at 323 K and a constant Seebeck coefficient of 15μV/mK^2.[36] In 2013, Toshima et al. also successfully hybridized PANI with Pt and Au nanoparticles. They used Poly(N-vinyl-2-pyrrolidone) (PVP)-protected Pt and Au nanoparticles (NPs) prepared by a conventional alcohol reduction method in the presence of PVP and mixed these PVP-protected metal NPs with PANI to prepare a hybrid material with a two-fold improvement in the thermoelectric figure-of-merit *ZT*.[37]

Despite the poor solubility and relatively low electrical conductivity of polythiophenes (PTH), a few studies have explored PTH-inorganic thermoelectric materials. PTH-Bi_2Te_3 nanocomposites were prepared by Casey et al. using a two-step method[38] where Bi_2Te_3 and PTH were prepared separately by hydrothermal synthesis and oxidative polymerization, respectively. A mixture of Bi_2Te_3 and PTH was subsequently prepared and pressed into a film in a graphite die (10 mm in diameter) under a pressure of 80 MPa. They studied the influence of temperature on performance properties and found that the highest electrical conductivity of 8 S/cm was achieved with a composite pressed at 623 K. This electrical conductivity value is nearly seven orders of magnitude greater than that of pure PTH. Unfortunately, this conductivity is still lower than that of bulk Bi_2Te_3

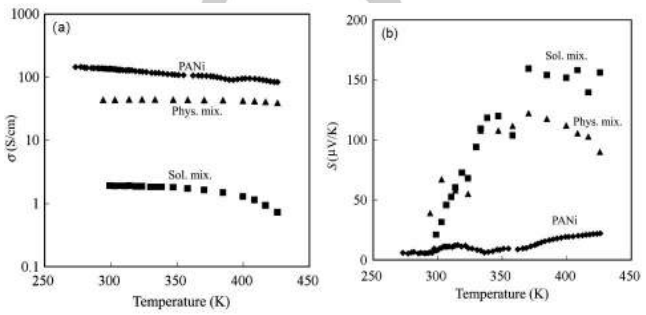

Figure 1. a) Electrical conductivity σ, b) Seebeck coefficient S of hybrid films prepared by physical mixing and solution mixing with a doped polyaniline film as a reference; adapted from Ref. [35].

pressed at 623 K, which is about 384 S/cm. It was also found that the optimal *ZT* value of PTH-Bi_2Te_3 nanocomposites could be achieved when the content of PTH in the composite is lower than 10 wt% and the sintering temperature is lower than 473 K.[39]

PEDOT conducting polymer has also attracted a lot of attention due to its high electrical conductivity, optical transparency, environmental stability, low density, flexibility, low thermal conductivity, and great thermal stability. However, it has limited solvent solubility and is often emulsified with polystyrene sulfonate (PSS) in water. As such, most of the related thermoelectric research focuses on improving the thermoelectric properties of PEDOT:PSS. Inorganic materials that are frequently mixed with PEDOT:PSS to form hybrids can be loosely classified into two categories: (1) carbon-based nanomaterials, and (2) metal-based chemicals such as Te nanorods, Bi_2Te_3, $Ca_3Co_4O_9$ compounds and Au noble metal nanoparticles.

Firstly, carbon nanotubes are often combined with PEDOT: PSS to achieve good thermoelectric performance. In 2008, Yu et al. proposed that the electrical conductivity could be dramatically increased by creating a network of carbon nanotubes (CNTs) in PEDOT:PSS composites while maintaining a constant thermal conductivity (Figure 2).[40] In 2010, Kim et al. prepared CNT-filled PEDOT:PSS composites and systematically investigated the influence of the type and concentration of inorganic constituents and the drying conditions on thermoelectric properties (Figure 3).[41] In their study, PEDOT:PSS particles were found to decorate the surface of the CNTs, bridging tube-tube junctions and allowing electrons to travel efficiently through the composites. Such a microstructure provides a high electrical conductivity (up to 400 S/cm at 35wt.% CNTs). Meanwhile, thermal transport across these tube-tube junctions is impeded due to a mismatch in vibrational spectra between the CNT and PEDOT:PSS. This property is ideal for developing high performance thermoelectric materials (high electrical conductivity and low thermal conductivity). The highest *ZT* (0.02) was obtained in composites containing 35 wt% single-wall CNTs. This performance may be further improved by increasing the electric conductivity of the polymer matrix by adding

filler materials with a high electrical conductivity such as carbon black, carbon fiber, or metallic carbon nanotubes.

Metal-based inorganic materials, which include Te nanorods, Bi_2Te_3, $Ca_3Co_4O_9$ powder and Au nanoparticles, all have large Seeback coefficients. In 2010 See et al. synthesized hybrids of Te nanorods and PEDOT:PSS with an in-situ process (see Figure 4)[42] to produce a film that possesses a continuous electrical network of nanoscale organic/inorganic interfaces. The electrical conductivity increased while the thermal conductivity diminished. The Seeback coefficient of the hybrids was found to be 144.1 μV/K, which is significantly greater than that of the polymer. Their study suggests that holes are the major charge carriers and charge transport does not exclusively occur through the PEDOT:PSS matrix. The high electrical conductivity achieved with these hybrid films (19.3S/cm) has been attributed to the improvement of interparticle contact as well as the prevention of Te nanorod oxidation by PEDOT:PSS. A high *ZT* of 0.1 was obtained at room temperature.

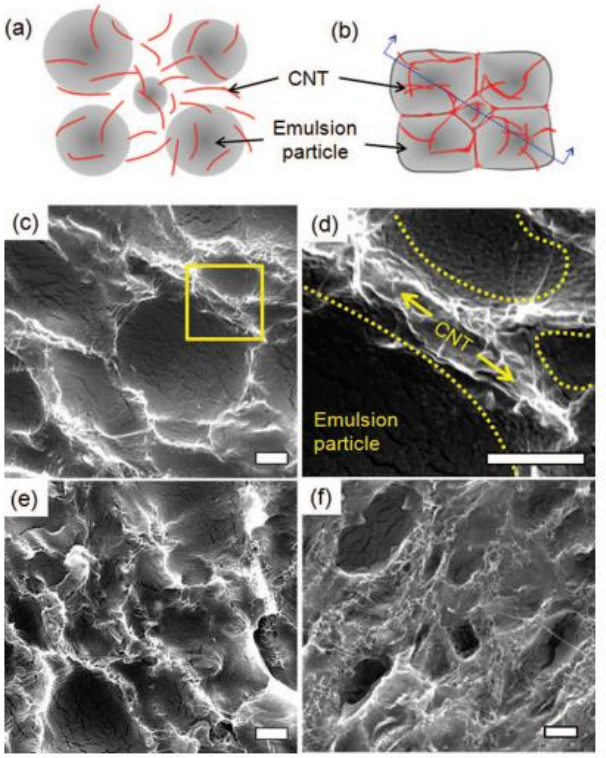

Figure 2. a) Schematic of CNTs suspended in an aqueous emulsion. Grey spheres and red lines represent emulsion particles and CNTs, respectively. b) Schematic of the emulsion-based composite after drying. The CNTs form a three-dimensional network along the surfaces of the spherical emulsion particles. SEM images of the cross-section of 5, 5, 10, and 20 wt% CNT composites are shown in panels c, d, e, and f respectively after the composites were freeze-fractured. All scale bars in the SEM images are 1μm; adapted from Ref. [40].

Zhang et al. found that the power factor of PEDOT:PSS can be enhanced by incorporating either p or n type Bi_2Te_3 powders into the composites due to the enhancement of the Seebeck coefficient and the electrical conductivity, respectively. These composites could be used for all-solution-processed thermoelectric devices deposited on flexible substrates (Figure 5).[43] Liu et al. successfully synthesized PEDOT:PSS/$Ca_3Co_4O_9$ composite films by mechanically blending $Ca_3Co_4O_9$ powder and a PEDOT:PSS solution (Baytron P) and casting the resulting mixture on polypropylene film substrates.[44] Results of both X-ray diffraction and scanning electron microscopy (SEM) (Figure 6) indicate that the $Ca_3Co_4O_9$ powders form into sheets and are well-incorporated with the PEDOT:PSS polymer. The Seebeck coefficient of the composite can be improved by increasing the $Ca_3Co_4O_9$ content; however, a decrease in electrical conductivity with increasing $Ca_3Co_4O_9$ content resulted in a decrease in the power factor.

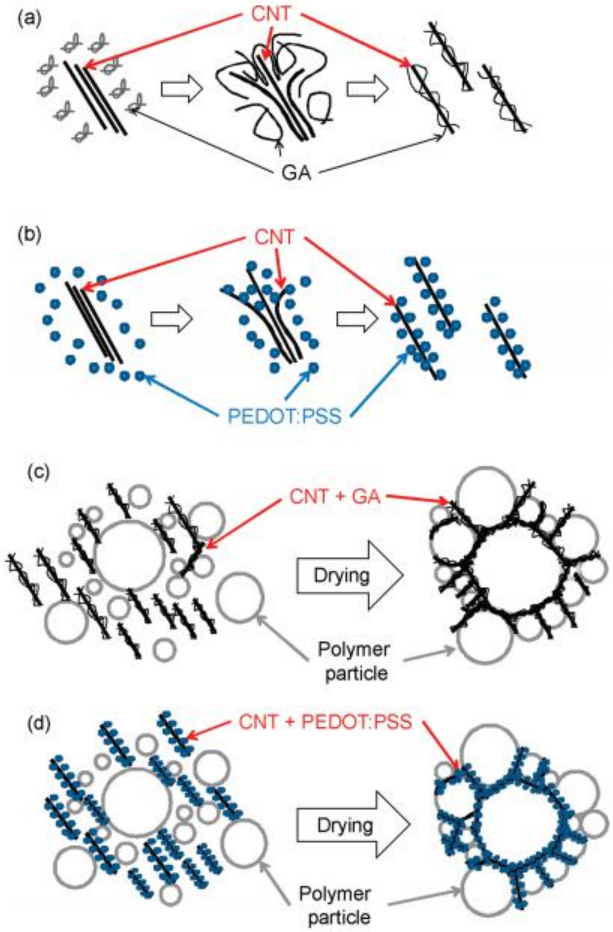

Figure 3. CNTs form a three-dimensional network along the surface of spherical emulsion particles. Panel a and b show schematics of CNTs dispersed by Gum Arabic (GA) and PEDOT:PSS, respectively. c) and d) show schematic illustrations of segregated-network formation before (left) and after (right) drying the water-based polymer emulsions; adapted from Ref. [41].

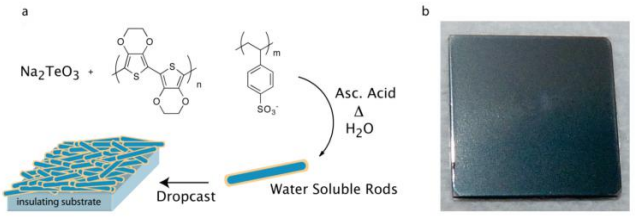

Figure 4. a) Synthesis of Te nanorods passivated by PEDOT:PSS followed by the formation of smooth nanocomposite films via solution casting. b) Picture of a typical drop-cast composite film on a 1 cm^2 quartz substrate illustrating the excellent film uniformity; adapted from Ref. [42].

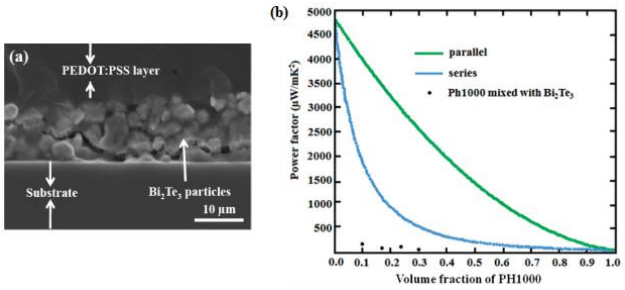

Figure 5. a) Cross section SEM of the PH1000 mixed with Bi_2Te_3 ball milled particles (30 % PEDOT:PSS by volume). b) Power factor of PH1000 mixed with p-type Bi_2Te_3 powders in parallel and series models. PH1000 is an aqueous dispersion of PEDOT/PSS which has almost the same electrical conductivity of commercialized TE ingot Bi_2Te_3; adapted from Ref. [43].

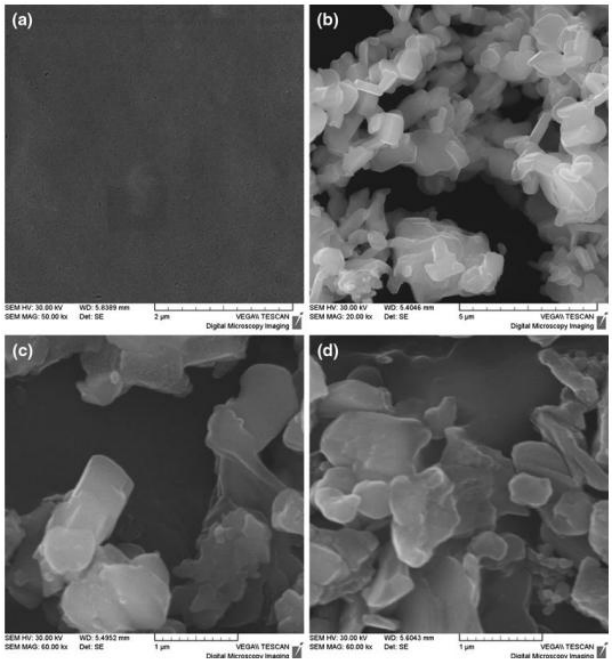

Figure 6. SEM images of a) a free-standing PEDOT-PSS film, b) neat $Ca_3Co_4O_9$ powder, and PEDOT:PSS/$Ca_3Co_4O_9$ composites prepared with a weight ratio of 10:5 c) and 10:8 d), respectively; adapted from Ref. [44].

Toshima et al. studied the effect of Au nanoparticles on the thermoelectric performance of PEDOT polymers. They prepared hybrid films of PEDOT:PSS with Au nanoparticles that were protected by two kinds of ligands (terthiophenethiol and dodecanethiol). The study revealed that a hybrid material composed of PEDOT and dodecanethiol-protected Au nanoparticles had an improved thermoelectric performance over pristine PEDOT. The electrical conductivity and *ZT* of the hybrids could be improved from 104 S/cm to 241 S/cm and from 0.62×10^{-2} to 1.63×10^{-2} at 323K, respectively.[45] They also reported that the Seebeck coefficient of hybrids composed of PEDOT:PSS and Au could be enhanced by varying the size and content of the 3-mercaptopropinoic acid stabilized gold (Au-MPA) nanoparticles.[46] They also suggested that the enhancement in the Seebeck coefficient is likely the result of a reduced carrier concentration due to the increased number of Au nanoparticles.

2.2 Metal-Organic Coordination Polymers

Metal-organic coordination polymers represent a class of metal coordination compounds where each metal centre binds to more than one ligand to create an array of metal centers. Linear coordination polymers consisting of transition metal ions and ethylenetetrathiolate (ett) are found to be highly efficient in achieving high electrical conductivity. These polymers do not enable bond rotation due to their ladder-like structure, making the polymer chains highly rigid to facilitate the extension of the conjugation system through the polymer chain and thereby improve intra-chain charge transport. Alvarez et al. have designed a planar ribbon composed of transition metal ions such as nickel, cobalt, and copper and ethylenetetrathiolate (ett), where 1D electrical conductivity is expected to emerge due to through bond-coupling between the metal d-orbitals and ligand π-orbitals.[47]

Most of metal coordinating compounds are completely insoluble in water and demonstrate either p- or n-type behavior. Usually the n-type metal moieties produce a higher *ZT* and power factor. In 2012, Sun et al. investigated the thermoelectric performance of a series of metal coordinating n-type and p-type polymers containing 1,1,2,2-ethylenetetrathiolate (ett) linking bridges: poly[(A_x(M-ett))](A = tetradecyltrimethyl ammonium, tetrabutyl ammonium, Na^+, K^+, Ni^{2+}, Cu^{2+}; M = Ni, Cu).[48] Both n-type and p-type organic thermoelectric materials including n-type poly[Na_x(Ni-ett)] and poly[K_x(Ni-ett)], and p-type poly[Cu_x(Cu-ett)] have demonstrated low thermal conductivities, and high electrical conductivities.[48] Their experimental results show that the two n-type materials have a high *ZT* value of 0.1 to 0.2 at a temperature of 400 K. By integrating n-type poly[Na_x(Ni-ett)] and p-type poly[Cu_x(Cu-ett)], a thermoelectric composite composed of n-p couples was produced which produced an output voltage of 0.26 V, a current of 10.1 mA, and a power factor of 2.8 µW cm^{-2} (see Figure 7). To date, it represents the best organic thermoelectric device ever reported under a temperature bias of 80 K. In a more immediate application, the n-p couple demonstrates great potential to serve as a thermoelectric refrigerator. In 2016, Sun and co-workers prepared flexible thin films of poly(nickel-ethylenetetrathiolate) with an electrochemical method which displayed highly promising n-type thermoelectric properties with a *ZT* value up to 0.3 at room temperature.[46] The results showed that the electrical conductivities of these thin films were four to five times higher than their powder counterparts while the Seebeck coefficients remained almost constant. The measured power factor values were above 453 µV/mK^2. The degenerate narrow-bandgap semiconductor behavior has been suggested to cause the coexistence of high electrical conductivity and high Seebeck coefficient in the coordination polymer. To date this is the largest room temperature power factor for an n-type organic thermoelectric material.

2.3 Organic-Inorganic Perovskite Materials

In recent years hybrid perovskites, such as $CH_3NH_3PbI_3$ and $CH_3NH_3SnI_3$, have been explored as efficient thermoelectric materials because of their large Seebeck coefficient and unusually low thermal conductivity. Owing to the fact that perovskite molecules can spontaneously crystallize via self-assembly processes, they do not require intricate equipment and can be synthesized and deposited by soft chemical methods at room temperature. The synthesis of perovskites can be generally divided into two steps: (1) synthesis of ammonium salts and (2) preparation of perovskite solution.

The thermal conductivity of single crystalline and polycrystalline organometallic perovskite $CH_3NH_3PbI_3$ was recently studied by Pisoni et al.[49] The thermal conductivity measured at room temperature was equal to 0.5 W/(mK) for single crystals and 0.3 W/(mK) for polycrystals. These values are quite low. The comparable absolute values and temperature dependence of the two samples' morphologies

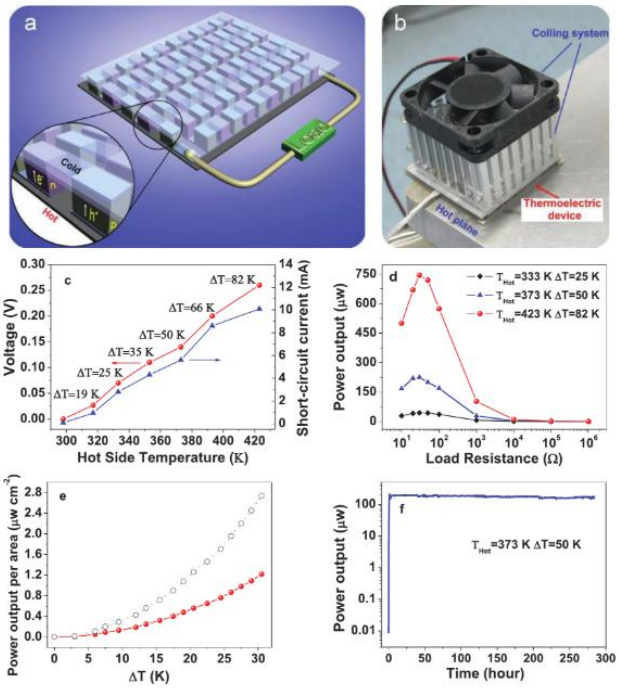

Figure 7. Thermoelectric module consisting of 35 thermocouples. a) Module structure, b) photograph of the module and the measurement system with hot plane and cooling fan, c) output and short-circuit current at various T_{hot} and ΔT d) measured power output of the module with different resistance loads, (e, solid circles) maximum power output per area of the module with the packing density defined as the occupied area of legs divided by the total device area, e), open circles) the extrapolated power output for a packing density of 0.94 g cm^{-3}, f) power output stability of the module operating with T_{hot} = 373K and ΔT=50 K; adapted from Ref. [48].

indicated the minor role of the grain boundaries on the heat transport. In 2015, Mettan et al. measured the thermoelectric properties of $CH_3NH_3PbI_3$ and $CH_3NH_3SnI_3$.[50] Their study showed that the *ZT* value of these compounds can be greatly enhanced with photo-induced doping of Pb into $CH_3NH_3PbI_3$ and chemical doping of Sn into $CH_3NH_3SnI_3$ to reach the performance level of the most efficient thermoelectric materials. The perovskite $CH_3NH_3SnI_3$ is even more advantageous as it is considered nontoxic and can be synthesized from solution allowing for cheap and large scale production.

Alongside experimental efforts, theoretical work has also been devoted to understanding the thermoelectric performance of these organic-inorganic hybrid perovskite materials. Through analysis of their electronic structures, theoretical work has provided insight into designing new types of thermoelectric materials. For example, He et al. employed density functional theory (DFT) and many body perturbation theory (MBPT) to evaluate the thermal transport properties of $CH_3NH_3PbI_3$ and $CH_3NH_3SnI_3$.[51] Their results indicated that materials with small effective masses of electrons and holes as well as relatively weak carrier-phonon interactions can have large carrier mobility values. The *ZT* values can range from 1 to 2 by tuning the carrier concentration values to the order of ~10^{-18} cm^{-3}, and the *ZT* values can be further improved by engineering the perovskite superlattices, to be more specific, by optimizing the lattice thermal conductivity.

In 2015, Lee et al. calculated the thermoelectric performance of organic-inorganic perovskite materials of type ABI_3 (A = CH_3NH_3, NH_2CHNH_2; B = Sn, Pb) using density functional theory (DFT) in which both the electron- and hole-doped materials were considered.[52] They calculated the *ZT* values of these perovskites using their crystal structures at room temperature (Figure 8) and compared them with those of well-known thermoelectric materials, such as Bi_2Te_3, under identical conditions. The chemical potential μ shown in Figure 9 for holes is defined as $\mu = E - E_{VBM}$, where $E < E_{VBM}$, and that for electrons by $\mu = E - E_{CBM}$ where $E > E_{CBM}$. From their calculations shown in Figure 9(d), it was found that the *ZT*s of electron-doped ABI_3 perovskites around 0.45 can be as large as that of hole-doped Bi_2Te_3 at room temperature. In contrast, the *ZT* values of hole-doped ABI_3 are around 0.35 lower than that of electron-doped ABI_3 (Figure 9d). Theoretical work by Filippetti et al. revealed that the *Z* value (*Z* is the slope of the line in figure power factor vs. thermal conductivity, defining the threshold of excellence for thermoelectric applications) of $CH_3NH_3PbI_3$ can reach as high as 1-3×10^{-3} K^{-1} by electron doping with materials possessing a moderate electrical conductivity (σ) and high Seebeck coefficient (*S*).[53] The study presented a route to achieving superior thermoelectric performance similar to the best performing thermoelectric tellurides and skutterudites ($CoAs_3$) available today.[53] They further proposed that the severely reduced thermoelectric performance of hole-based carriers compared to electron-based carriers is primarily due to the smaller band anisotropy of the holes.

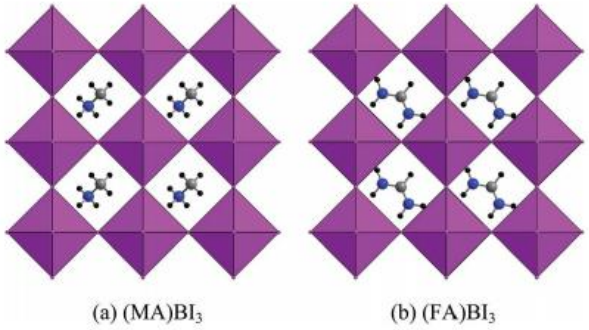

Figure 8. Projection views of organic-inorganic hybrid perovskites along the c-axis (Out of the page): a) $(MA)BI_3$ and b) $(FA)BI_3$, where M = Pb, Sn. MA = methyl ammonium ($CH_3NH_3^+$), and FA = formamidinium ($HC(NH_2)_2^+$). The blue, grey and black circles represent the N, C and H atoms, respectively, and purple octahedral units represent the BI_6 octahedra. The C-N axis of MA and the N⋯N axis of FA cations are oriented within the page to show their chemical structures; adapted from Ref. [52].

In order to further examine other factors influencing thermoelectric performance of ABI_3 perovskite materials. Shuai and co-workers studied the thermoelectric performance of $CH_3NH_3PbI_3$ based on first-principles calculations and took both the impurity scattering and acoustic phonon scattering into consideration. In Boltzmann transport theory, electrical conductivity, thermal conductivity and Seebeck coefficient are all determined by the relaxation time of charge carriers, which is inverse of the scattering probability of charge carriers by phonons and impurities. Their calculation showed that the thermoelectric transport coefficients of Poly(3,4-ethylenedioxythiophene)-tosylate (PEDOT:Tos) agree with experimental data after factoring in the impurity scattering and acoustic phonon scattering.[54] The results show that the tetragonal phase of $CH_3NH_3PbI_3$ has superior thermoelectric properties over the cubic phase due to its higher carrier mobility and lower thermal conductivity. The p-type $CH_3NH_3PbI_3$ can reach a high *ZT* value of 1.26 at 330 K (Figure 10). Moreover, they thought that the hole-doped $CH_3NH_3PbI_3$ exhibited higher thermoelectric performance than the electron-doped type, in contrast to the conclusions by Filippetti et al. Such differing conclusions demonstrate the complexity and degree of unexplored

aspects in perovskite composite processing, electronic structure, and simulation.

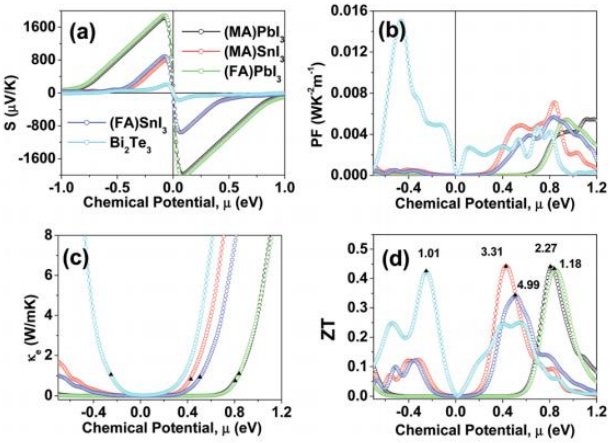

Figure 9. Calculated transport coefficients for ABI_3-type organic-inorganic hybrid perovskites as a function of the chemical potential μ: a) the Seebeck coefficients *S*, b) the power factor $S^2\sigma$, c) the electronic thermal conductivity (κ_e, is the electron thermal conductivity arising from charge carriers), and d) the figure of merit *ZT*. The filled triangles in c) indicate the κ_e leading to a maximum *ZT*. Numbers at the peaks in d) refer to the carrier concentrations (in units of 10^{19} cm^{-3}). The zero chemical potential refers to the midpoint of the band gap; adapted from Ref. [52].

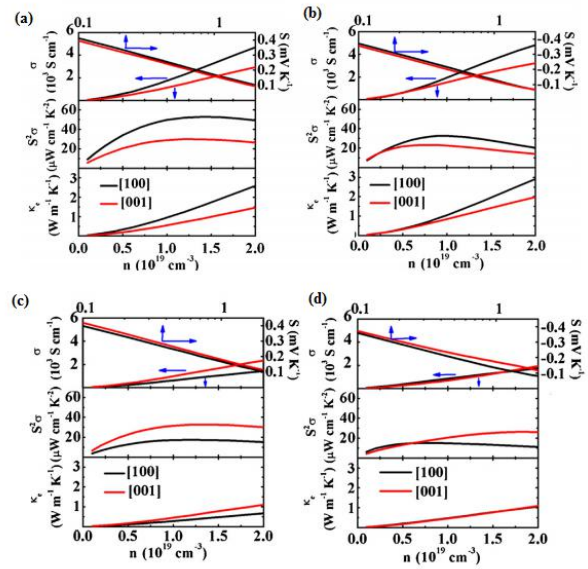

Figure 10. Electrical conductivity σ, Seebeck coefficient *S*, power factor $S^2\sigma$, and electronic thermal conductivity κ_e of tetragonal $CH_3NH_3PbI_3$ at 330 K as a function of hole a) and electron b) concentration; and cubic $CH_3NH_3PbI_3$ at 330 K as a function of hole c) and electron d) concentration. The black and red lines represent the [100] and [001] transport directions, respectively; adapted from Ref. [54].

Concerning phase effects on the improvement of thermoelectric properties, Wang et al. measured the thermal conductivities of methylammonium lead iodide ($MAPbI_3$) in different phases (cubic, tetragonal, and orthorhombic) using equilibrium molecular dynamics simulations (Figure 11).[55] They found that the thermal conductivity of $MAPbI_3$ is dependent on the phase, and temperature. By adjusting these two variables together, it is possible to find a wide temperature range over which the materials show ultralow thermal conductivity (less than 1 W/mK).

In addition, they also made qualitative estimates of the thermal conductivities of various mixed perovskites $MABX_3$ (B = Pb, Sn; X=I, Br). It was found that the Br- and Sn-based $MABX_3$ perovskites had higher thermal conductivities than I- and Pb-based perovskites (Figure 12). Therefore, $MAPbI_3$ perovskites possessing ultralow thermal conductivities can have a high thermoelectric figure of merit and serve as an excellent thermoelectric material.

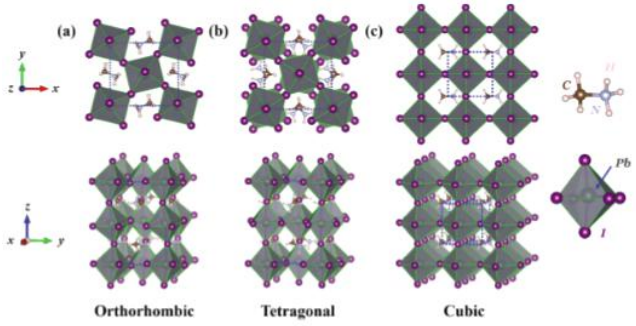

Figure 11. Atomistic configuration of a) orthorhombic, b) tetragonal, and c) cubic phases of $CH_3NH_3PbI_3$ ($MAPbI_3$). The dashed blue cuboids represent the unit cell in each phase. The transparent dark grey octahedra denote the cages formed by six I^- ions around one Pb^{2+} ion; adapted from Ref. [55].

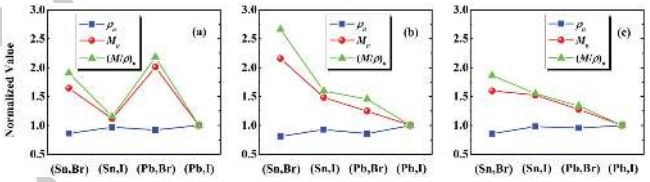

Figure 12. Normalized values of mass density ρ_n, averaged elastic property $M_n = (E_n+G_n)/2$, and their ratio $(M/\rho)_n$ for different $MABX_3$ formulations in a) orthorhombic, b) tetragonal, and c) cubic phases (B = Pb, Sn; X = I, Br). The values of E, G, and the lattice constants are obtained from DFT calculations; adapted from Ref. [55].

3. Strategies for Enhancing the Thermoelectric Performance of Hybrid Organic-Inorganic Nanocomposites

Generally, three approaches have been employed to increase the electrical conductivity and reduce thermal conductivity of organic-inorganic hybrids for achieving outstanding thermoelectric performance: (1) Controlling the inorganic nanostructure such as size, dimension and mophorlogy is favored for *ZT* enhancement; (2) Modifying the organic materials remarkably improves the electrical conductivity through doping or controlling the oxidation state of the organic polymer; and (3) Engineering the interfaces within the material efficiently increases the power factor by improving the independent Seeback coefficient of the hybrids.

3.1 Controlling the Nanostructure of the Inorganic Component

It is understood that certain changes in a material's nanostructure can lead to an increase in the Seebeck coefficient due to quantum confinement effects while also reducing the thermal conductivity due to greater scattering of phonons at the interfaces. Consequently, the

thermoelectric performance of the inorganic components can be effectively manipulated by controlling their particular nanostructure. For example, the reduction in dimensionality can play an important role in decreasing the thermal conductivity due to the increased phonon scattering at the larger number of interfaces afforded by low dimensional materials as compared to their bulk equivalents. Therefore, low dimensional materials have attracted a great deal of attention. A theoretical study by Hicks et al. first suggested that miniaturization would affect thermoelectric properties once the quantum regime is reached to enable an enhancement in the figure of merit *ZT*. In such a study, the calculated *ZT* of bismuth telluride showed a dramatic increase when reducing the dimensionality from 3D (bulk, $ZT = 0.52$ at 300 K) to 2D (thin films or superlattices, $ZT = 6.9$ at 300 K).[56] Recently, they experimentally confirmed the effect of quantum confinement in the density of states on the thermoelectric figure of merit, *ZT* in 2D superlattices.[57]

3.1.1 Three-dimensional nano-structured bulk materials (NBM):

NBMs can combine the superior thermoelectric performance of low dimensional materials with the production of large-scale bulk samples, making them easier to handle and shape. It provides a way to increase the scattering of phonons without strongly affecting charge transport. This effect produces a lower thermal conductivity in the lattice over a wide temperature range.[58] For example, Dresselhaus et al. have shown that the heterogeneous nanoparticle compounds or those with nanoparticle inclusions had better thermoelectric performance than an alloy of the two constituents.[59]

Bi_2Te_3 was one of the first materials to be transferred into a bulk nanostructure in order to raise its *ZT*.[60] Through milling high purity powders of Bi and Te in a 2:3 ratio and then compressing via spark-plasma sintering, disk shaped Bi_2Te_3 samples were obtained possessing a *ZT* value of 1.2 at 150 °C. Scheele and co-workers developed a two-step approach to prepare Bi_2Te_3 nanoparticles with sizes smaller than 10 nm (see Figure 13).[61] Their unique two-step synthetic route utilizes bismuth nanoparticle intermediates. The intermediates were synthesized using oleylamine as a reducing agent together with 1-dodecanethiol as the stabilizer. The as-prepared bismuth nanoparticles were then treated with a Tellurium solution in trioctylphosphine to get a bismuth-tellurium alloy. Ultrafine powder of $Bi_xSb_{2-x}Te_3$, was prepared by hot pressing yielding a *ZT* value of 1.4 at 100 °C.[62] This value increased to 1.56 at 30 °C when the nano-structured $Bi_{0.52}Sb_{1.48}Te_3$ bulk material was subjected to melting, quenching, annealing, and spark-plasma sintering.[63] Theoretical studies showed that optimization of the ratios of the individual constituents can lead to further improvement. A compound of composition $Bi_{0.5}Sb_{1.5}Te_3$ was found to have a *ZT* value as high as 1.8 at 27 °C.[64]

Among other inorganic thermoelectric materials, nano-structured PbTe exhibits a *ZT* of 0.7 at 400 °C. Heremans et al. Fabricated PbTe-based high-*ZT* alloys containing EuTe inclusions (a coarse-grained sample was obtained by ball milling for one hour and a fine-grained sample was obtained by ball milling for 22 hours).[65] Both nanostructured samples displayed an enhancement in S over that of the bulk PbTe. However, the coarse-grained sample containing EuTe showed no enhancement while the fine-grained version of this sample showed a 10%-15% increase in thermopower. Such parallel experiments allow researchers to conclude that the thermopower enhancement comes from the PbTe nanostructure not the EuTe inclusion. PbTe can also be modified by adding an excess of lead nanoparticles (diameter of 30 nm), which also lead to an increase in the Seebeck coefficient compared to bulk PbTe.[66,67] In 2011, several studies reported *ZT* values as large as 1.8 in PbTe-PbS alloys (525 °C)[68] and in PbTe-PbSe alloys (575 °C).[69] The significant improvement in the *ZT* value may be attributed to the reduction of the thermal conductivity of the nanostructured materials. In addition to the above binary alloy, ternary alloys such as $AgSbTe_2$ have also been

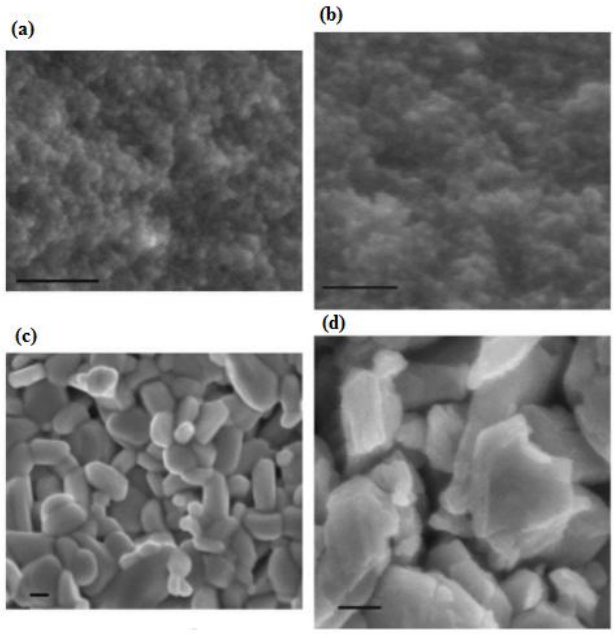

Figure 13. The morphology of Bi_2Te_3 nanoparticles before (a and b) and after thermal treatment (c and d). All scale bars are equal to 100 nm; adapted from Ref. [61].

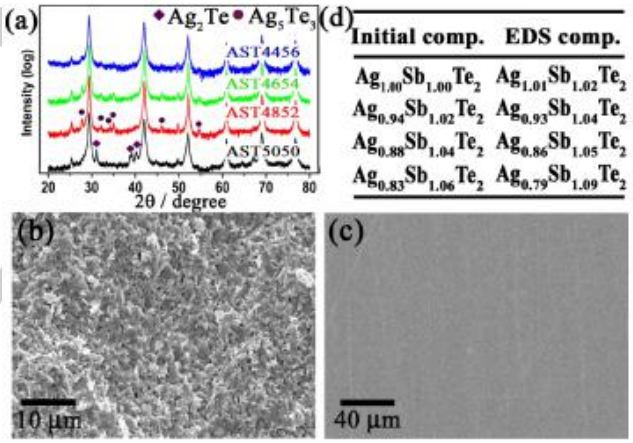

Figure 14. a) XRD pattern of samples with different compositions after annealing. b) Cross-sectional scanning electron microscopy image of an $AgSbTe_2$ sample. c) Polished surface of $AgSbTe_2$ for energy dispersive spectroscopy (EDS) study with no large pores observed. d) EDS composition of different samples after annealing; adapted from Ref. [70].

explored as thermoelectric materials. Interestingly, $AgSbTe_2$ is often found mixed with other compounds, such as SiGe (named TAGS, with a *ZT* of 1.2 at 150 °C), rather than being used on its own. Wang et al. succeeded in preparing $AgSbTe_2$ ternary alloy using mechanical alloying and spark-plasma-sintering techniques to obtain a *ZT* value of 1.59 at 300 °C. The great performance has been attributed to the extremely low thermal conductivity of 0.3 W/mK and a large Seebeck coefficient of 260 μV/K at room temperature (Figure 14).[70] Du and co-workers further improved the *ZT* value of $AgSbTe_2$ to 1.65 at 300 °C by introducing 5-10 nm nanopores to the bulk materials, which are in

situ generated during a melt-spinning spark-plasma-sintering synthesis process (Figure 15).[71]

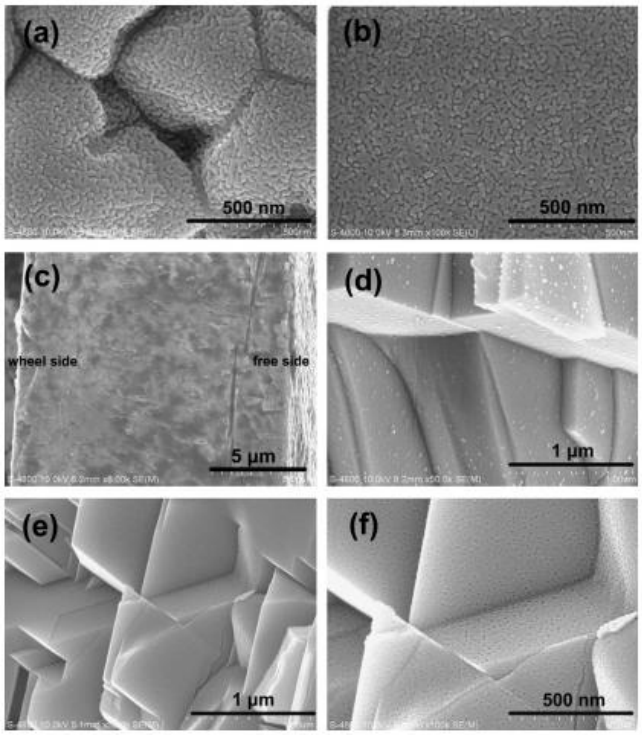

Figure 15. Field-effect scanning electron microscopy (FESEM) photographs of $AgSbTe_2$ ribbons: a) free side; b) wheel side; c) cross-section; d) SPS (the samples prepared by spark plasma sintering methods); and MS-SPS (the bulk materials yielded by grounding the ribbon shaped samples into powder and sintered by SPS); e) low magnification; f) high magnification; adapted from Ref. [71].

$AgSbTe_2$ has also been incorporated with the well-known thermoelectric material PbTe to form a new material designated as LAST (Lead, Antimony, Sliver and Tellurium, $AgPb_mSbTe_{2+m}$). Kanatzdis and co-workers reported that $AgPb_mSbTe_{2+m}$ with m = 10 and 18 can exhibited a large thermoelectric figure of merit (ZT = 2.1) at 530 °C.[72] Subsequent research used mechanical alloying and spark-plasma sintering to prepare LAST with reported ZT values between 1.5 and 1.7.[73] Variation in the ZT value may be related to changes in the ratio of each constituent in the alloy which not only highlights the importance of the chemical composition but also justifies further research on this promising thermoelectric material. However, three dimensional materials limit their applications in high thermoelectrical performance due to their low efficiency in using interfacial quantum confinement. Two or even lower dimensions need to be investigated.

3.1.2 Two Dimensional Thin Films and Superlattices:

In 1993, Hick and Dresselhaus put forward the idea that the ZT value ($S^2\sigma T/k$) of certain materials could be increased by forming them into quantum-well superlattice structures (i.e., thin films).[73] Their calculation indicates that using Bi_2Te_3 with a quantum-well structure which is made into a particular orientation can increase the ZT by 13 times relative to the bulk structure due to the reduction of phonon thermal conductivity caused by phonon scattering between layers. In 1997, Venkatasubramanian et al. fabricated layers of Bi_2Te_3 and Sb_2Te_3 with periods from 1 to 8 nm via metal organic chemical vapor deposition (MOCVD).[74] These films were c-oriented (along the growth direction) and were bonded to each other by van der Waal forces preventing bismuth and antimony from inter-diffusing to different layers (see Figure 16). The reported ZT value was 2.0 at 27 °C, and subsequently enhanced up to 2.4 by controlling the transport of phonons and electrons in the thin-film thermoelectric materials at the same temperature.[75]

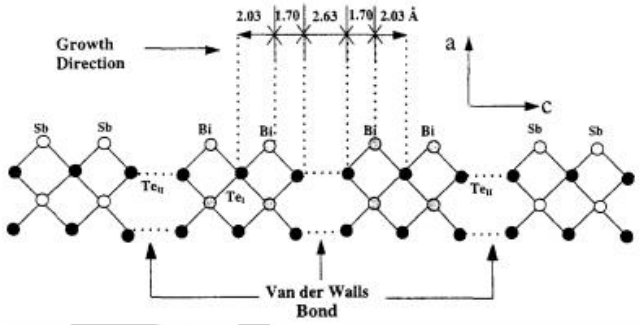

Figure 16. Crystal structure of Bi_2Te_3/ Sb_2Te_3 materials layered along the growth direction. Note the presence of van der Waals-like bonding along the c-axis; adapted from Ref. [75].

Other extensively studied superlattices include lead salt films such as $PbTe/PbSe_{0.2}Te_{0.8}$,[76] $PbTe/Pb_{0.93}Eu_{0.07}Te$ quantum-wells,[57] and Si/Ge superlattices.[75-77] For these two-dimensional materials, the enhancement of the figure of merit has generally been attributed to the reduction of their thermal conductivity. Experiments have shown that the room temperature thermal conductivity measured in the in-plane direction decreases with decreasing superlattice period and that a stronger reduction is produced in the through-thickness direction. For example, Lee et al. investigated the thermal conductivity of Si/Ge superlattices with superlattice periods between 30 and 300 Å and found the thermal conductivity to be below that of conventional Si/Ge alloys.[77] In 2000, Borca-Tasciuc et al. measured the thermal conductivity of Si/Ge superlattices and got similar results (Figure 17).[78] Zeng et al. reported the fabrication and characterisation of single-element thin film superlattice SiGe/Si coolers which show a two-fold performance improvement. that is, the improvement is attributed to the reduced thermal conductivity and the increased thermoelectric emission cooling due to the large thermal spread of carriers near the Fermi energy.[79]

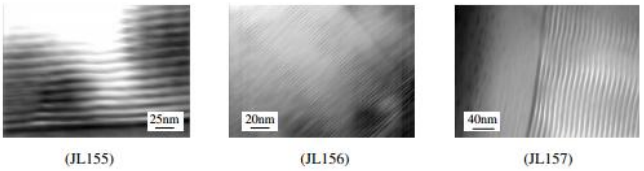

Figure 17. TEM images of undoped Si/Ge superlattices. The period of the superlattice JL155, JL156 and JL157 are 140Å, 44Å and 90Å, respectively; adapted from Ref. [79].

3.1.3 One Dimensional Nanowires and Nanotubes:

The advantage of 1D nanostructures is that when the diameter of the nanowires and nanotubes are sufficiently small, the electronic density of states are concentrated at certain energies. Thus, reducing the size of nanowires to house just a few quantum states cause a split in the energy bands that give rise to discrete sub-bands. In this way, a semiconductor can behave like a semimetal, leading to the reduction in

lattice thermal conductivity without impacting electronic properties. To date, there is little data on figures of merit for one-dimensional thermoelectric materials. This likely stems from challenges involved in assembly and measurement due to the small size and inhomogenity.

The thermoelectric performance of isolated nanowires has been measured with suspended micro-chips,[80] or by using the Harman method in which only resistance measurements by both DC and AC methods are required to obtain the *ZT* values. *ZT* values of 200 nm Bi_2Te_3 wires around 0.82 were reported.[81] Compared to Bi_2Te_3 wires, an even higher *ZT* value can be achieved by silicon nanowires which were studied both experimentally and computationally by Boukai et al., exhibiting a 100-fold increase (*ZT* = 1 at 300 K) over bulk Si (*ZT* = 0.01 at 300 K).[82,83] Bismuth telluride nanowire arrays, prepared through electrodeposition, have been recently reported to have a *ZT* value of 0.9 at 353 K (see Figure 18).[84] It was also observed that the figure of merit might decrease with time due to the possible formation of oxidation layers on the nanowire surface. When the diameters of these nanowires are not small enough to achieve quantum confinement, any observed improvement in the figure of merit likely stems from a reduction in the thermal conductivity. In the quantum confinement regime, an increase in the Seebeck coefficient should also be observed.

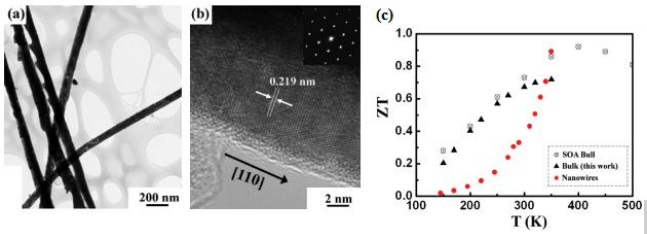

Figure 18. a) TEM image of Bi_2Te_3 nanowires. b) HRTEM image of a single Bi_2Te_3 nanowire. Inset: Diffraction patterns of a selected area showing lattice spacing. c) Temperature dependence of *ZT* for nanowire and bulk formulations; adapted from Ref. [84].

3.1.4 Zero Dimensional Quantum Dots:

As suggested by corresponding studies,[57,84,85] lowering the dimensionality of a material can lead to greater quantum confinement and cause an increase in the Seebeck coefficient. Meanwhile, the increase in phonon scattering as a result of lower dimensionality reduces the thermal conductivity. A combination of improved Seebeck coefficient and lowered thermal conductivity is expected to lead to significant improvement in the thermoelectric performance. As such, there has been growing interest in fabricating materials with zero dimensionality in the last decade as if will likely show further increases in the Seebeck coefficient and further reductions in the thermal conductivity. For example, Harman et al. investigated PbTe/Te superlattices produced by the addition of a nanometer thick layer of Te atoms on top of the PbTe layer prior to barrier layer addition. They found that the *ZT* increased from 0.37 for homogeneous PbTe to 0.52 for the PbTe/Te superlattice at room temperature due to the formation of PbTe/Te quantum dots on the surface.[84] They further investigated the thermoelectric properties of $PbSe_xTe_{1-x}$/PbTe quantum-dot superlattices and observed great enhancement of the Seebeck coefficient as well as the overall *ZT* as a result of the quantum confinement effects on the electronic density of states. In their experiments, the measured *ZT* value is almost double that of the best value reported for bulk PbTe (see Figure 19).[85]

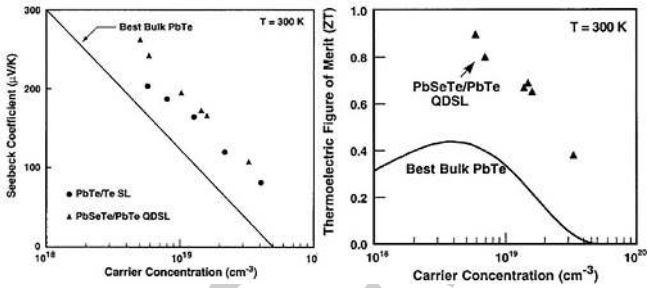

Figure 19. A new PbSeTe/PbTe quantum dot superlattice structure and its seebeck coefficient, thermoelectric figure of merit vs. carrier concentration; adapted from Ref. [85].

3.2 Modification of Organic Materials

The low electrical conductivity, which is a shortcoming of organic thermoelectric materials, can be significantly improved through doping or controlling the oxidation state of the organic polymer.[86,87] For example, by controlling its oxidation level Bubnova et al.[86] were able to greatly improve the power factor of a conductive polymer PEDOT:p-toluenesulfonate (PEDOT:Tos). Their study shows that when the PEDOT:Tos polymer was reduced, which caused a drop in charge carrier concentration in the film, the film conductivity exhibited a dramatic change. It decreases from 300 S/cm at 36% oxidation down to 6×10^{-4} S/cm at 15% oxidation (see Figure 20(a)). An optimized *ZT* of 0.25 was obtained at room temperature at 22% oxidation (Figure 20(b)). Kim et al.[87] used a large number of non-ionized dopants (dimethyl sulfoxide (DMSO) and ethylene glycol (EG)) to modulate the carrier mobility. In their study, a PEDOT:PSS solution was first mixed with EG or DMSO and then spin-coated on a glass substrate. After thermal annealing, the doping treatment was applied by immediately immersing the samples in an EG bath (kept at 60 °C for EG-mixed PEDOT:PSS) and at room temperature for DMSO-mixed PEDOT:PSS for a certain length of time to control the doping level. A maximum *ZT* value of 0.42 was realized for DMSO-doped PEDOT:PSS at room temperature and 0.28 for EG-doped PEDOT:PSS.

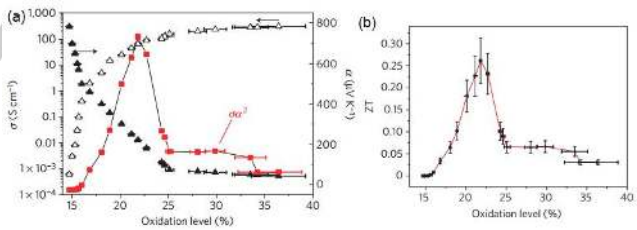

Figure 20. a) Seebeck coefficient *S* (filled triangles), electrical conductivity σ (open triangles) and corresponding power factor (red squares) versus oxidation level. b) The values of *ZT* at room temperature for various PEDOT:PSS oxidation levels (assuming that the thermal conductivity of PEDOT:Tos is constant and equals 0.37 W/mK); adapted from Ref. [86].

It is interesting to point out that while the electrical conductivity of the PEDOT:PSS was enhanced when doped with dimethylsulfoxide (DMSO), there is no reduction in the Seebeck coefficient. Such a behavior is likely due to the unique conducting nature of PEDOT:PSS upon doping with DMSO, exhibiting a hopping transport-dominated regime to a carrier scattering-dominated regime.[88] The study showed that the power factor of this new thermoelectric material can exceed 100 $\mu W/mK^2$.This is nearly five orders of magnitude greater than that of pure PEDOT:PSS (Figure 21).

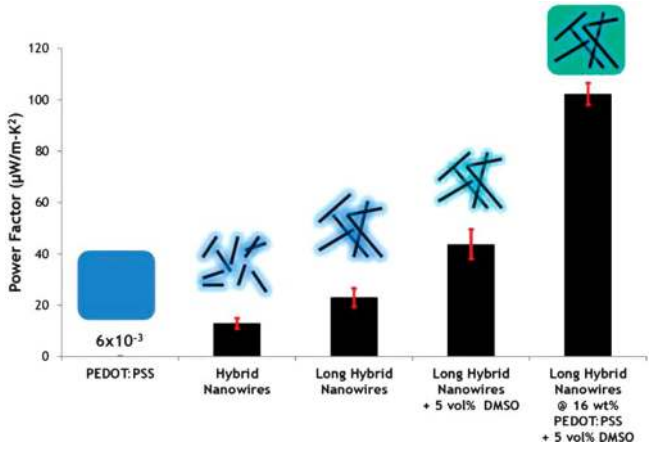

Figure 21. Power factor values for various hybrid organic-inorganic formulations composed of doped PEDOT:PSS and Te nanowires. A five orders of magnitude improvement in the power factor over pure PEDOT: PSS is obtained by introducing hybrid PEDOT:PSS-Te nanowires, and finely tuned by the addition of high conductivity PEDOT: PSS infused with a polar solvent (DMSO); adapted from Ref. [88].

Another effective approach for improving the thermoelectric performance involves changing the typical coil structure of a conductive polymer into an extended linear structure. For example, Wang et al. used carbon nanotubes as the platform to synthesize regularly spaced Polyaniline (PANI)/Carbon nanotube (CNT) composites (Figure 22).[89] The CNTs were embedded in the PANI/CNT nanofibers and oriented along the fiber axis due to the strong chemical interaction between PANI and CNTs. The composites exhibited improved electrical properties because the linear structure of the PANI improved electron delocalization leading to increased charge mobility. Improving the crystallinity of a conducting polymer is also an effective method for improving its thermoelectric properties. Cho et al. synthesized single-crystal PEDOT nanowires using liquid-bridge-mediated nano-transfer printing (LB-nTM) with vapor phase polymerization (VPP).[90] As illustrated in Figure 23, the LB-nTM-VPP method starts with the formation of single-crystal PEDOT nanowires from 3,4-ethylenedioxythiophene monomers that are self-assembled

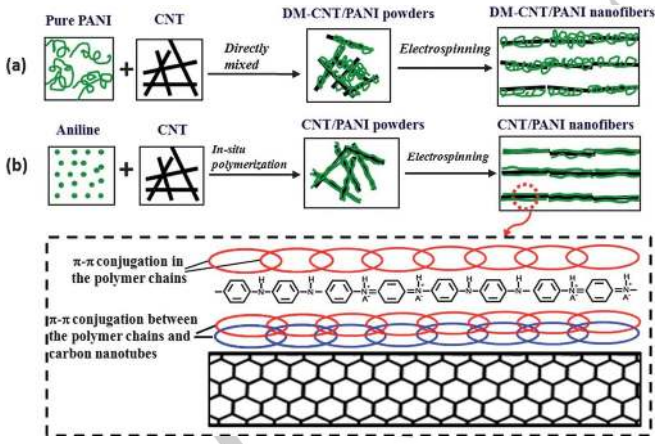

Figure 22. Schematic representations of the formation mechanism of DM-CNT/PANI (a) and CNT/PANI (b) nanofibers; adapted from Ref. [89].

and crystallized during the vapor phase polymerization process withinnanoscale channels of a mold. These PEDOT nanowires are then directly transferred to specific positions on a substrate to generate a nanowire array by a direct printing process.[93] The conductivity of these single-crystal PEDOT nanowires averages 7619 S/cm with peak values of 8797 S/cm. This value exceeds those reported in the literature for PEDOT nanostructure/thin films which range from 2 S/cm to 4500 S/cm.[43-46]

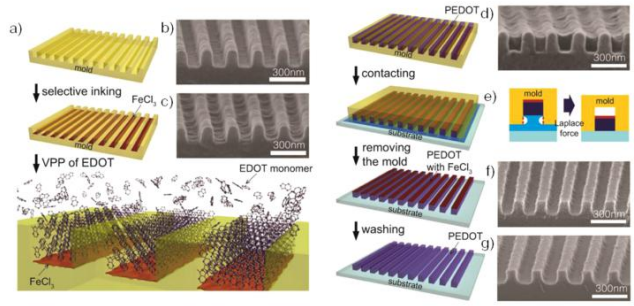

Figure 23. Fabrication of single-crystal PEDOT nanowire arrays. a) Schematic illustration of the procedure used to fabricate single-crystal PEDOT nanowire arrays on a substrate using liquid-bridge-mediated nano-transfer printing with vapor phase polymerization. b) SEM image of a polyurethane acrylate (PUA) mold with a nanoscale pattern. c) SEM image of the mold filled with $FeCl_3$ catalyst molecules. d) SEM image of the mold filled with single-crystal PEDOT nanowires grown via the VPP process. e) Schematic illustration of a liquid bridge formed by a polar liquid layer between PEDOT nanowires and a substrate. f) SEM image of a single-crystal PEDOT nanowire array on a Si substrate before washing. g) SEM image of a single-crystal PEDOT nanowire array on a Si substrate after washing with methanol to remove residual $FeCl_3$; adapted from Ref. [90].

3.3 Interfacial Engineering of Organic-Inorganic Hybrid Materials

Organic and inorganic materials have very different electronic densities and wave functions at their surface. The interface produced during the combination of two components is expected to play a critical role in determining the overall electrical and thermoelectric properties of the hybrid organic-inorganic thermoelectric materials. The charge carrier filtering effect produced by the energy level mismatch between the inorganic and organic components increases the power factor by improving the independent Seeback coefficient of the hybrids. Du et al. prepared a Bi_2Te_3-based alloy of p-type $Bi_{0.5}Sb_{1.5}Te_3$ nanosheets through an intercalation and exfoliation approach (The lithium ions intercalated $Bi_{0.5}Sb_{1.5}Te_3$ suspension in an ethylene glycol solution, and $Bi_{0.5}Sb_{1.5}Te_3$ powder was readily exfoliated into nanosheets), and subsequently synthesized PEDOT:PSS hybrids via drop casting and spin coating (Figure 24).[91] The power factor was increased to 32.26 $\mu W/mK^2$; three times that of single phase PEDOT:PSS. The composite films also showed electrical conductivities as high as 1295.21 S/cm, a great improvement over dimethyl sulfoxide-doped PEDOT:PSS films (753.8 S/m) and Bi_2Te_3-based alloy bulk materials (850-1250 S/cm). This research demonstrates that the thermoelectric efficiency can be maximized by tuning the organic-inorganic interface by controlling parameters such as the roughness and thickness of the films. In general, high surface roughness leads to stronger carrier scattering and quantum confinement effect, and therefore a high Seebeck coefficient.

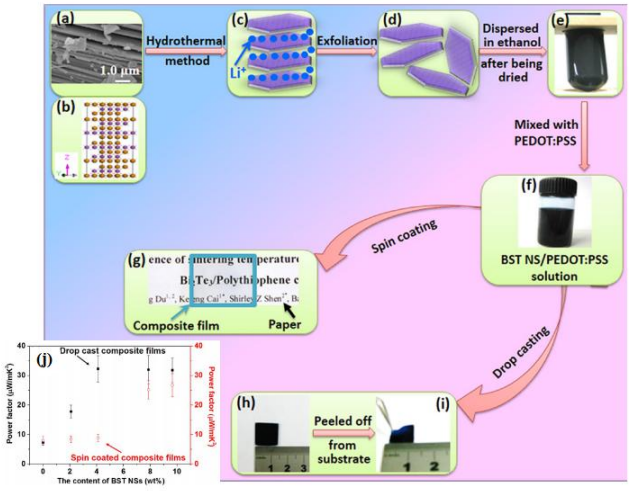

Figure 24. Illustration of the preparation steps for BST NS ($Bi_{0.5}Sb_{1.5}Te_3$ nanosheet)/PEDOT: PSS films. a) Typical FESEM image of the BST ingot after grinding. b) Crystal structure of Bi_2Te_3 (yellow: Te, Purple: Bi). c) Li-intercalated units after hydrothermal treatment. d) BST NSs after exfoliation. e) BST NSs dispersed in ethanol. f) BST NS/PEDOT: PSS solution. g) Spin coated BST NS/PEDOT: PSS film on glass substrate (marked by a dark blue square). h) Drop cast BST NS/PEDOT: PSS film on a glass substrate. i) Drop cast BST NS/PEDOT: PSS film after being peeled off the glass substrate. j) Power factor calculated for the drop cast and the spin coated films as a function of the BST NS content in the composite films; adapted from Ref. [91].

Ju et al. synthesized SnSe nanosheets from a bulk SnSe ingot by hydrothermal lithium-intercalation followed by exfoliation. SnSe nanosheet/PEDOT:PSS composites with varying SnSe nanosheet content were prepared by a solution-processable fabrication method. The figure of merit of the fabricated hybrid was markedly enhanced to 0.32 at a SnSe nanosheet loading of 20 wt% (Figure 25).[92] The power factor enhancement is also found to depend on the SnSe nanosheet content. This dependence is attributed to the influence of nanosheet content on the total interface. In 2016 Ju et al. also investigated DMSO-treated SnSe/PEDOT: PSS nanosheets[93] The results indicated that the thermal conductivity was insensitive to the addition of SnSe nanosheets. The electrical conductivity σ is determined by the equation $\sigma = ne\mu$, where n, e and μ are the carrier concentration, charge per carrier, and carrier mobility, respectively. The experimental results indicate the n values decreased as the content of SnSe nanosheets increased. This is likely due to the potential barriers in between SnSe and PEDOT:PSS that originate from the energetic mismatch at the interfaces. As a result, the electrical conductivity decreased with increasing SnSe nanosheet content while the Seebeck coefficient

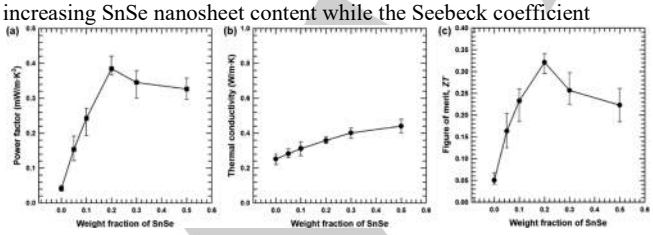

Figure 25. a) Power factor, b) thermal conductivity, and c) *ZT* of SnSe NS/PEDOT: PSS composites with varying SnSe NS content; adapted from Ref. [92].

gradually increased under larger nanosheet loading. An increased power factor up to 386 μW/mK^2 was observed with 20 wt.% SnSe nanosheet content. The measured performance is roughly 257 times higher than that of pristine PEDOT:PSS films (~1.5 μW/mK^2).

To further benefit from the influence of interfacial conditions on performance properties, Choi et al. synthesized a ternary hybrid composite graphene/polymer/inorganic nanocrystal (reduced graphene oxide (rGO)/PEDOT: PSS/tellurium nanowires (TeNWs)).[94] This ternary hybrid contains two types of energy barriers (0.24 eV at the Te/PEDOT:PSS interface, and 0.31 eV at the graphene/PEDOT:PSS interface) (Figure 26). Such a configuration has two heterojunctions at rGO/PEDOT:PSS and PEDOT:PSS/TeNW with controlled interfacial energy barriers that can significantly enhance the electrical conductivity without causing a significant decrease in the Seebeck coefficient. The ternary hybrids show a power factor of 143 μW/mK^2, a much higher performance value when compared to the single phase Te NW materials (1.26 μW/mK^2) and PEDOT:PSS/TeNW (9.33 μW/mK^2).

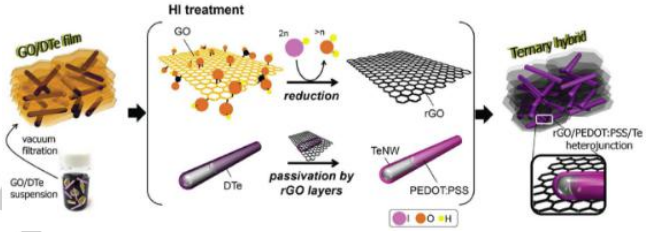

Figure 26. Schematic illustration of a thermoelectric hybrid reduced graphene oxide (rGO)/PEDOT: PSS/tellurium nanowires (TeNWs) paper; adapted from Ref. [94].

3.4 Improving the Thermal Conductivity of Hybrid Materials

Discovery of low-thermal conductivity materials for the thermoelectric applications has proven quite challenging. To achieve low thermal conductivity, Yang et al. recently designed a kind of all-inorganic halide perovskites $CsSnI_3$ with an ultralow thermal conductivity (~0.4 W/mK) without scarifying their original high electrical conductivity.[95] Later on, hybrid organic-inorganic halide perovskites $CH_3NH_3PbX_3$ (X = Cl, Br, I) have been successfully constructed with an even lower thermal conductivity (0.22-0.36 W/mK),[96] due to the occurrence of resonant scattering between organic cations and inorganic framework. Other related metal-organic framework $TCNQ@Cu_3(BTC)_2$ (TCNQ = tetracyanoquinodimethane, BTC = benzene tricarboxylate) also showed a very low thermal conductivity of 0.27 ± 0.04 W/mK,[97] which is even better than conducting polymers.[98] It is likely derived from the disorder of molecules in the pores and other phonon scattering. These works demonstrate that the thermal conductivity of thermoelectric materials can be tailored and optimized by the synthesis of new kind of hybrid and supramolecular materials.

4. Hybrid Organic-Inorganic Thermoelectric devices

Thermoelectric conversion devices can convert heat directly into electricity thus providing a means of recovering waste heat for power generation and refrigeration. In order to minimize the cost of the energy obtained by thermoelectric devices, it is necessary to find a way to develop more efficient thermoelectric materials. Significant progress has been made in constructing high performance thermoelectric devices which will be introduced in the following sections.

4.1 Hybrid Organic-Inorganic Hybrid Thermoelectric Power Generator (TEG)

TEG, also called a Seebeck generator, can directly convert thermal energy generated from natural heat sources or ubiquitous waste heat into electricity. Thermoelectric power generation generally requires three essential components: thermoelectric material, thermoelectric module, and systems that interface with the heat source. The thermoelectric materials generate electricity while under a temperature gradient. In general, TEGs are simple, compact, robust, and very reliable because they contain no moving parts. Flexibility in the thermoelectric component is also crucial to ensure tight conformity to the surface of the heat source and maximize collection of any waste heat. This is especially important for heat sources with irregular surfaces. Recently, there has been growing interest in self-powered wearable electronics such as smart watches, wrist bands, smart glasses and e-skins; materials that require power but also generate heat that is not easily captured. The growth in popularity of such technologies has prompted much interest in flexible TEGs as detailed below.

Suemori et al. reported a flexible and lightweight TEG fabricated on a polyethylene naphthalate film substrate.[99] The thermoelectric material used in this new TEG is a composite material consisting of CNTs and polystyrene. The device had a power flux-density of 55 mW/m^2 at a temperature difference of 343 K. Experimental results indicate that the TEG is lightweight (15.1 mg/cm^2) due to the voids in the composite and can endure mechanical deformation to high degrees of bending. In 2014, We et al. prepared a high performance flexible TEG module using a screen-printed inorganic thermoelectric thick film and organic conducting polymer hybrid composite.[100] Specifically, a 40 μm-thick thermoelectric film consisting of a Bi_2Te_3 film as the n-type component and a Sb_2Te_3 film as the p-type component was screen-printed on a highly flexible polyimide film substrate. The film was subsequently annealed at 450 °C under N_2 atmosphere. There are many pores in the screen-printed thermoelectric thick film due to the evaporation of solvent and organic binder in the paste during the annealing process. The sample was then coated by a PEDOT:PSS solution while dimethyl sulfoxide was also added in order to improve the electrical conductivity. The TEG module fabricated with these materials can produce a power flux-density of 1.2 mW/cm^2 under a 50 K temperature difference.

Thermoelectric materials containing hybrid metal-organic Cu(I)-ethylenetetrathiolate were used by Shen and co-workers to construct TEG.[101] They found that the performance of the thermoelectric material could be optimized by controlling the oxidation level of the materials. The study demonstrates that reduction can improve the electrical conductivity and lower the Seebeck coefficient, and subsequently enhance the power factor to 118.2 $\mu W/mK^2$ and *ZT* to 0.060 at 400 K. Next, they fabricated a TEG with 220 pairs of thermocouples based on this Cu(I)-ethylenetetrathiolate material as the p-type material and poly[K_x(Ni-ett)] as the n-type material. A 5 nm thick polydimethylsiloxane membrane (50 mm × 50 mm) containing 440 equally separated cavities was used as a support for the thermoelectric legs. The I-V curve of the device at a temperature difference of 60 K is shown in Figure 27. The device produced an open circuit voltage of 1.51 V, a short circuit current of 2.71 mA under a temperature difference of 60K, and a maximum output power over 1 mW. This power output is the best thermoelectric performance based on organic thermoelectric materials.

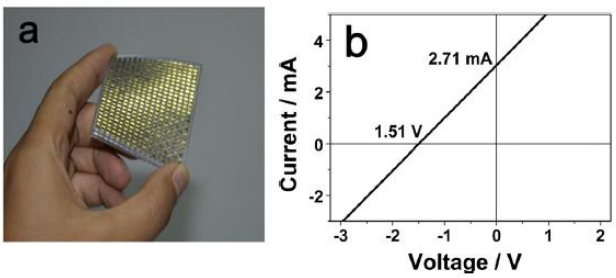

Figure 27. a) Photograph of the polydimethylsiloxane membrane with the n-type and p-type legs imbedded in it. b) I-V curve of the TEG device with 220 pairs of thermocouples (Cu(I)-ethylenetetrathiolate as p-type material and poly[K_x(Ni-ett)] as n-type material) under a temperature difference of 60 K; adapted from Ref. [101].

TEG built by Hewitt et al. utilized pristine single walled carbon nanotubes as the p-type layers and polyethylenimine (PEI) doped single walled carbon nanotubes as the n-type layers.[102] The modules constructed in this study are composes of three unique sublayers (p-type, n-type, and insulator) that combine to form individual thermocouples in the final module. Polyvinylidene fluoride (PVDF) is chosen as the base polymer for all three unique sublayers since it is readily soluble in the solvents used for dispersing carbon nanotubes. PVDF is water insoluble which aids in the durability and versatility of the final module. No hole dopant was required for the p-type sublayers since the carbon nanotubes typically become oxygen doped during synthesis thus conferring p-type behavior. For the n-type sublayers, an additional electron donor was required, and PEI has been shown to be an effective dopant by adsorbing onto and coating the walls of the nanotubes and donating the lone pair electrons from the amine groups within the repeating units of PEI. The resulting device consisting of nine 5 thermocouple modules connected electrically in series and thermally in parallel produced a Seebeck coefficient of 96 ± 4 μV/K and an output power of 14.7 nW per thermocouple at a temperature difference of 50 K. These values are 6.3 times and 44 times higher than previously reported multilayered carbon nanotube composite devices, respectively. Their research suggests the potential use of such devices in the area of lightweight and flexible electronics applications.

Similar to the design of Hewitt et. al., Zhou et al. fabricated a compact, and efficient flexible thermoelectric module based on single walled carbon nanotubes (SWNT) as a p-type film and PEI-doped SWNTs as an n-type film.[103] As shown in Figure 28, in the first step a large-area CNT film with a thickness of ~3 μm was cut into a 96 mm × 10 mm stripe and placed on an ultrathin polyethylene terephthalate (PET) (2 μm in thickness) substrate on which thin PET double-sided adhesive tape was alternately adhered as a mask. They found that the p-type SWNT films can be directly switched to n-type films by drop-casting the solution of PEI in ethanol. Different doping levels were achieved by varying the concentration of PEI solution from 0.01 to 5 wt.% that was applied to the SWNT ribbons. In the next step, a solution of 1 wt.% PEI in ethanol was drop-casted into the unprotected areas and dried at 50 °C in air for 5 minutes. As a result, the unshaded areas in the CNT films are converted into n-type regions and the areas covered by PET double-side adhesive tape remained p-type. The results indicated that the Seebeck coefficient of the PEI-doped SWNT ribbon turned to a negative value of -16 μV/K, indicating switching from a p-type to an n-type region. The optimum n-type power factor (~1500μW/mK) was obtained at a PEI concentration of 1 wt.% with a high electrical conductivity of 3.63×105 S/m, high Seebeck coefficient of -64 μV/K. Moreover, the synthesized n-type SWNT film exhibited outstanding stability with less than 5% variation in the electrical conductivity and Seebeck coefficient during the test period of 3 months. This module produced an open-circuit voltage of 11.3 mV, a short-circuit current of 0.9 mA, a maximum output power of 2.51 μW, and a power flux-density of 167 $\mu W/cm^2$ at a temperature difference of 27.5 K.

A radial TEG design composed of Te nanowires in PEDOT/PSS as the p-type material and poly[K_x(Ni-ett)]/PVDF/DMSO as the n-type material was reported by Menon et al.[104] Because of the low-cost, lightweight, and flexibility of the paper-based device, calligraphy was

used to directly coat the p-type and n-type polymer inks onto the 1×1 cm^2 papers until they were saturated. The samples were then dried for 30 minutes in an oven at 60 °C to remove excess solvent. The papers were subsequently cut into paper disks with an inner radius (r_{in}) of 6.5 mm and an outer radius of (r_{out}) of 35 mm and secured on a glass plate to prevent wrinkling. The disks were then dried at 70 °C for 30 minutes in an oven. Once dry, the second side of each disk was coated with the same material and dried as before. For the obtained radial TEG consisting of 15 n-p thermocouples, an output voltage of 85 mV and a power flux-density of 15 nW/cm^2 were produced without the need for active cooling at a temperature difference of 40K. These values are higher than those of reported devices with the same number of couples.[105,106] Both the p-type and n-type paper-based composites showed a reduced thermal conductivity and enhanced Seebeck coefficient as compared to pristine samples. This led to the high performance of the designed radial TEG design (shown in Table 1). Moreover, this high performance polymer TEG has applications beyond waste-heat recovery in the areas of wearable electronics and self-powered sensors requiring low costs per unit power.

To further improve the efficiency of TEGs, a flexible thermoelectric device based on a new TiS_2/hexylamine superlattice film was fabricated by Tian et al.[107] In their previous research, they synthesized the TiS_2/hexylamine hybrid and found that its electrical resistance was unaffected by bending,[108] and the electrical conductivity of the composite film was enhanced to 756 S/cm from the 300 S/cm of the pristine TiS_2 crystal. This can be attributed to the increase in change transfer from the organic molecules. The outstanding thermoelectric performance and flexibility of TiS_2/organic superlattice films motivated the subsequent research into their use in flexible thermoelectric devices. One of the devices consists of 5 pairs of thermoelectric couples employing ethylene glycol-treated PEDOT:PSSas the p-type material and TiS_2/hexylamine superlattice film as the n-type material. Both materials were deposited onto the PET substrate to retain flexibility. An output voltage of 33 mV could be obtained with a maximum power flux-density of 2.5 W/m^2 over a temperature difference of 70 K. Notably, the power density is 1-2 orders of magnitude higher than that of thermoelectric modules reported earlier.[109-111] This significant progress is encouraging for the future of thermoelectric devices. Specifically, with the development of new thermoelectric materials and new TEG designs, efficient devices can be built for a broad range of applications including as a promising source of power in wearable electronics.

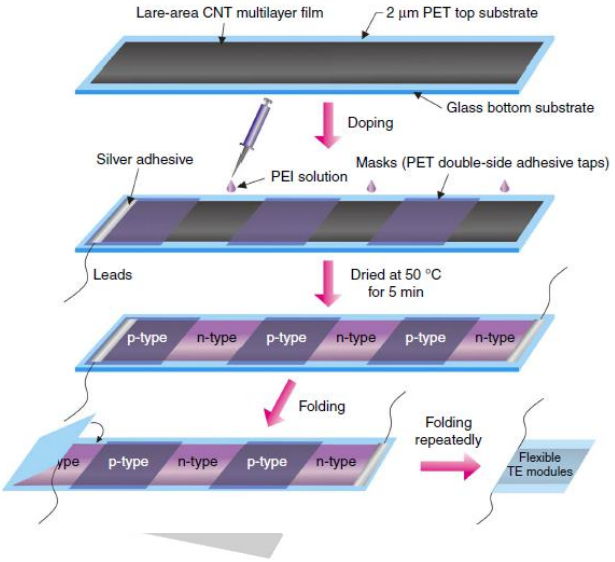

Figure 28. Schematic summarizing the fabrication of a novel, compact, and efficient flexible thermoelectric module based on large-area continuously synthesized CNT films and localized PEI doping; adapted from Ref. [103].

Table 1. Thermoelectric properties of polymer and polymer-paper based TEGs at room temperature (295K)

	S (μV/K)	Σ (S/cm)	$S^2\sigma$ (μW/mK^2)
p-type PEDOT/PSS with Te nanowires			
Pristine (thin film)	109.1±8.6	4.2±0.5	4.9±0.6
On paper	204.1±19.8	(4.9±0.6)×10^{-3}	(2.1±0.4) ×10^{-2}
n-type poly[Kx(Ni-ett)] with PVDF/DMSO			
Pristine (thin film)	-34.7±3.1	12.6±0.7	1.5±0.1
On paper	-28.3±1.5	0.5±0.06	(4.1±0.5)×10^{-2}

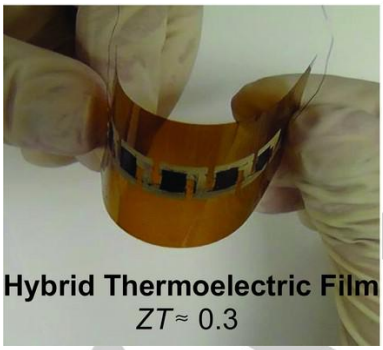

Figure 29. The high thermoelectric performance of (dimensionless thermoelectric figure-of-merit, $ZT \approx 0.3$, based on the thermal conductivity through the film) a flexible five-leg thermoelectric device composed of three-component n-PETT/CNT/PVC hybrid films and Ag electrodes on a polyimide substrate; adapted from Ref. [111].

4.2 Thermoelectric Coolers (TEC)

Thermoelectric cooling uses the Peltier effect to create a heat flux between the junction of two different types of materials. With the consumption of electrical energy, a solid state thermoelectric heat pump transfers heat from one side of the device to the other, depending on the direction of the current. Compared to traditional refrigeration, thermoelectric coolers have many advantages including no moving parts (i.e. no vibration), simplicity, long life and flexible shape. Sun et al.[48] combined n-type poly[Na_x(Ni-ett)] and p-type poly[Cu_x(Ni-ett)] to construct a thermoelectric device composed of 35 n-p couples. Their device showed promising performance as a thermoelectric cooler (output voltage of 0.26 V, a current of 10.1 mA, and a power flux-density of 2.8 μW/cm^2 under a temperature bias of 80 K). Toshima et al. constructed a five-couple thermoelectric hybrid device based on a three-component hybrid material composed of nanodispersed poly(nickel 1,1,2,2-ethenetetrathiolate) (n-PETT), carbon nanotubes (CNTs) and poly(vinyl chloride) (PVC).[112] The three-component n-

PETT/CNTs/PVC hybrid films are usually prepared by drop-casting the mixed dispersion of n-PETT, CNTs and PVC in N-methyl-2-pyrrolidone (NMP) at the designated ratios on a quartz or polyimide substrate. The films were slowly dried in air on a hot plate at 60 °C for 12 h. And the devices consisted of five thermocouples with a three-component hybrid film and a Ag electrode. The relations between the output voltage, power, and electric current are summarized in Figure 29. The maximum power was found to be 3.88 μW under a temperature bias of 100 K.

Thermoelectric coolers (TECs) have found applications in things as small as a beverage cooler, and as large as a submarine or railroad car. Unfortunately, TECs have a limited lifetime which can be measured by the change in their AC resistance (ACR). When a TEC gets "old" or worn out, the ACR will increase. New high-performance materials for thermoelectric cooling are being actively pursued.[108]

4.3 Thermoelectric sensor

Thermoelectric principles have also been utilized to make gas sensors by detecting heat signals produced during gas phase reactions.[113-116] For example, in 2001 Shin et al. designed a thick film NiO-based H_2 sensor in which half the surface was coated by a thin layer of Pt upon which reaction with H_2 occurred. The heat produced by the reaction creates a hot region enabling a thermoelectric voltage to form between the hot and cold regions of the film thus indicating the presence of H_2.[117] Such film-based gas sensors have shown sufficient sensitivity and response time, and have great applicability in gas alarms and fuel gas control systems.

5. Summary and Perspective

In summary, remarkable achievements have been realized in the last decade in the development of high performance thermoelectric materials. The above detailed discussions suggest that thermoelectric materials with improved *ZT* values must be developed in order to allow thermoelectric technologies to be adopted for a broad range of practical applications and to ultimately become more competitive in the race to find alternative energy sources and develop new ways of benefiting from existing energy sources (energy capture). Controlling the electrical transport properties (Seebeck coefficient, *S*, and electrical conductivity, σ) as well as the thermal transport properties (κ) are important areas that can enable larger *ZT* values. In the last decade, many outstanding thermoelectric materials have been prepared in an organic-inorganic hybrid manner. Generally, there are three typical approaches to enhance the thermoelectric properties of organic-inorganic hybrids: (1) Controlling the inorganic nanostructure and dimensionality. By constructing zero dimensional quantum dots, one dimensional nanowires and nanotubes, two dimensional thin films and superlattices, and even three dimensional nano-structured bulk materials, one can increase the Seebeck coefficient (*S*) by capitalizing on quantum confinement effects and reducing the thermal conductivity (κ) by taking advantage of the greater phonon scattering at the interfaces. (2) Modifying the organic materials. It has been demonstrated that the thermoelectric performance of organic materials can be improved by doping. Doping can maximize the thermoelectric power factor because it determines free-carrier concentration and carrier mobility both of which dictate electrical conductivity. Another effective approach for improving thermoelectric performance involves changing the typical coil structure of organic polymeric materials into an extended linear structure. (3) Engineering the interfaces within the material. The nature of the interface produced during the combination of organic and inorganic components is critical to determining the overall thermoelectric properties. In addition to the selection of organic and inorganic materials that have suitable differences in their work functions, methods to control the electron density at the interface and defect population within the material are essential. Depending on the structural composition and the alignment of organic components at the interface, the charge transport mechanism can vary.

Based on our understanding of these efforts and related theoretical work, future research should be centered on three particular areas: (1) discovering new suitable thermoelectric materials with intrinsically high *ZT* values; (2) developing ways of decoupling *S* and σ, while also increasing them simultaneously; and (3) pushing lattice thermal conductivity κ_L toward the amorphous limit. Although challenges still exist, particularly the laws of physics require the electronic part of thermal conductivity (k) to be proportional to electrical conductivity thus limiting the simultaneous enlargement of *S* and σ, recent progress in this field has established a strong foundation for the further development of highly efficient thermoelectric materials. Many more improvements and innovations are expected and required in the established but also burgeoning field of thermoelectric materials.

Acknowledgements

We are grateful for financial support from the National Natural Science Foundation of China (51772219, 51872209, 21471116, 21628102, and 61728403), the Zhejiang Provincial Natural Science Foundation of China (LZ18E030001, LZ17E020002 and LZ15E020002).

Keywords: organic-inorganic interfaces • electronic structures • thermal conductivity • energy conversion • thermoelectrics

References

[1] H. Goldsmid in *Thermoelectric refrigeration*, Springer, **2013**, pp. 10-20.
[2] Q. Zhang, Y. Sun, W. Xu, D. Zhu, *Adv. Mater.* **2014**, *26*, 6829-6851.
[3] C. L. Wan, X. K. Gu, F. Dang, T. Itoh, Y. F. Wang, H. Sasaki, M. Kondo, K. Koga, K. Yabuki, G. J. Snyder, R. G. Yang, K. Koumoto, *Nat. Mater.* **2015**, *14*, 622-627.
[4] B. C. Sales, *Science* **2002**, *295*, 1248-1249.
[5] L. E. Bell, *Science* **2008**, *321*, 1457-1461.
[6] Q. Jin, S. Jiang, Y. Zhao, D. Wang, J. H. Qiu, D. M. Tang, J. Tan, D. M. Sun, P. X. Hou, X. Q. Chen, K. P. Tai, N. Gao, C. Liu, H. M. Cheng, X. Jiang, *Nat. Mater.* **2019**, *18*, 62-68.
[7] A. Boyer, E. Cissé, *Mater. Sci. Eng. B* **2009**, *13*, 103-111.
[8] X. Ji, B. Zhang, T. M. Tritt, J. W. Kolis, A. Kumbhar, *J. Electron. Mater.* **2007**, *36*, 721-726.
[9] G. J. Snyder, E. S. Toberer, *Nat. Mater.* **2008**, *7*, 105-114.
[10] A. Majumdar, *Science* **2004**, *303*, 777-778.
[11] M. Bharti, A. Singh, S. Samanta, D. K. Aswal, *Prog. Mater. Sci.* **2018**, *93*, 270-310.
[12] C. C. Lin, Y. C. Huang, M. Usman, W. H. Chao, W. K. Lin, T. T. Luo, W. T. Whang, C. H. Chen, K. L. Lu, *ACS Appl. Mater. Interfaces* **2019**, *11*, 3400-3406.
[13] K. Hiraishi, A. Masuhara, H. Nakanishi, H. Oikawa, Y. Shinohara, *Jpn. J. Appl. Phys.* **2009**, *48*, 071501-071504.
[14] Y. Shinohara, Y. Isoda; Y. Imai, K. Hiraishi, H. Oikawa, H. Nakanishi, *International Conference on Thermoelectrics* **2007**, IEEE, 405-407.

[15] K. C. Chang, M. S. Jeng, C. C. Yang, Y. W. Chou, S. K. Wu, M. A. Thomas, Y. C. Peng, *J. Electron. Mater.* **2009**, *38*, 1182-1188.
[16] J. Y. Kim, J. H. Jung, D. E. Lee, J. Joo, *Synth. Met.* **2002**, *126*, 311-316.
[17] B. Russ, A. Glaudell, J. J. Urban, M. L. Chabinyc, R. A. Segalman, *Nat. Rev. Mater.* **2016**, *1*, 16050.
[18] H. L. Wang, M. X. Wang, C. Qian, X. K. Hong, D. B. Zhang, Y. S. Liu, X. F. Yang, *Phys. Lett. A* **2017**, *381*, 1738-1744.
[19] Y. Du, S. Z. Shen, K. Cai, P. S. Casey, *Prog. Polym. Sci.* **2012**, *37*, 820-841.
[20] D. Y. Chung, T. Hogan, P. Brazis, M. Rocci-Lane, C. Kannewurf, M. Bastea, C. Uher, M. G. Kanatzidis, *Science* **2000**, *287*, 1024-1027.
[21] C, G. Wu, D. C. DeGroot, H. O. Marcy, J. L. Schindler, C. R. Kannewurf, Y. J. Liu, W. Hirpo, M. G. Kanatzidis, *Chem. Mater.* **1996**, *8*, 1992-2004.
[22] H. Anno, K. Yamaguchi, T. Nakabayashi, H. Kurokawa, F. Akagi, M. Hojo, N. Toshima, *Materials Science and Engineering* **2011,** 1638-1640.
[23] B. Zheng, Y. Liu, B. Zhan, Y. Lin, J. Lan, X. Yang, *J. Electron. Mater.* **2014,** *43*, 3695-3700.
[24] B. Zheng, Y. Lin, J. Lan, X. Yang, *J. Mater. Sci. Technol.* **2014**, *30*, 423-426.
[25] H. Anno, M. Fukamoto, Y. Heta, K. Koga, H. Itahara, R. Asahi, R. Satomura, M. Sannomiya, N. Toshima, *J. Electron. Mater* **2009**, *38*, 1443-1449.
[26] S. R. Hostler, P. Kaul, K. Day, V. Qu, C. Cullen, A. R. Abramson, X. F. Qiu, C. Burda, 10th Intersoc. Conf. **2006**, 1400-1405.
[27] X. B. Zhao, S. H. Hu, M. J. Zhao, T. J. Zhu, *Mater. Lett.* **2002**, *52*, 147-149.
[28] Y. Li, Q. Zhao, Y. Wang, K. Bi, *Mater. Sci. Semicond. Process.* **2011**, *14*, 219-222.
[29] N. Toshima, M. Imai, S. Ichikawa, *J. Electron. Mater.* **2010**, *42*, 898-902.
[30] H. Liu, J. Wang, X. Hu, R. I. Boughton, S. Zhao, Q. Li, M. Jiang, *Chem. Phys. Lett.* **2002**, *352*, 185-190.
[31] Q. Yao, L. Chen, W. Zhang, S. Liufu, X. Chen, *ACS Nano* **2010**, *4*, 2445-2451.
[32] C. Meng, C. Liu, S. Fan, *Adv. Mater.* **2010**, *22*, 535-539.
[33] Y. Y. Wang, K. F. Cai, J. L. Yin, B. J. An, Y. Du, X. Yao, *J. Nanopart. Res.* **2011**, *13*, 533-539.
[34] Y. Li, Q. Zhao, Y. G. Wang, K. Bi, *Mater. Sci. Semicond. Process.* **2011**, *14*, 219-222.
[35] N. Toshima, I. Masahiro, I. Shoko, *J. Electron. Mater.* **2011**, *40*, 898-902.
[36] N. Toshima, N. Jiravanichanun, H. Marutani, *J. Electron. Mater.* **2012**, *41*, 1735-1742.
[37] N. Toshima, *Pure Appl. Chem.* **2013**, *85*, 437-451.
[38] Y. Du, K. F. Cai, Z. Qin, S. Z. Shen, P. S. Casey, *MIME* **2011**, 462-465.
[39] Y. Du, K. F. Cai, K. F. Cai, B. An, Z. Qin, P. S. Casey, *J. Mater. Sci.: Mater. Electron.* **2012**, *23*, 870-876.
[40] C. Yu, Y. S. Kim, D. Kim, J. C. Grunlan, *Nano Lett.* **2008**, *8*, 4428-4432.
[41] D. Kim, Y. Kim, K. Choi, J. C. Grunlan, C. H. Yu, *ACS Nano* **2010**, *4*, 513-523.
[42] K. C. See, J. P. Feser, C. E. Chen, A. Majumdar, J. J. Urban, R. A. Segalman, *Nano Lett.* **2010**, *10*, 4664-4667.
[43] B. Zhang, J. Sun, H. E. Katz, F. Fang, R. L. Opila, A*CS Appl. Mater. Interfaces* **2010**, *2*, 3170-3178.
[44] C. C. Liu, F. X. Jiang, M. Y. Huang, B. Y. Lu, R. R. Yue, J. K. Xu, *J. Electron. Mater.* **2011**, *40*, 948-952.
[45] N. Toshima, N. Jiravanichanun, H. Marutani, *J. Electron. Mater.* **2012**, *41*, 1735-1742.
[46] N. Toshima, N. Jiravanichanun, *J. Electron. Mater.* **2013**, *42*, 1882-1887.
[47] S. Alvarez, R. Vicente, R. Hoffmann, *J. Am. Chem. Soc*. **1985**, *107*, 6253-6277.
[48] Y. Sun, P. Sheng, C. Di, F. Jiao, W. Xu, D. Qiu, D. B. Zhu, *Adv. Mater.* **2012**, *24*, 932-937.
[49] A. Pisoni, J. Jaćimović, O. Barišić, M. Spina, R. Gaál, L. Forró, E. Horvath, *J. Phys. Chem. Lett.* **2014**, *5*, 2488-2492.
[50] X. Mettan, R. Pisoni, P. Matus, P. Pisoni, J. Jaćim, B. Náfrádi, M. Spina, D. Pavuna, L. Forró, E. Horvath, *J. Phys. Chem. C* **2015**, *119*, 11506-11510.
[51] Y. He, G. Galli, *Chem. Mater.* **2014**, *26*, 5394-5400.
[52] C. Lee, J. Hong, A. Stroppa, M. H. Whangbo, J. H. Shim, *RSC Adv.* **2015**, *5*, 78701-78707.
[53] A. Filippetti, C. Caddeo, P. Delugas, A. Mattoni, *J. Phys. Chem. C* **2016**, *120*, 28472-28479.
[54] T. Zhao, D. Wang, Z. Shuai, *Synth. Met.* **2017**, *225*, 108-114.
[55] M. Wang, S. Lin, *Adv. Funct. Mater.* **2016**, *26*, 5297-5306.
[56] L. D. Hicks, M. S. Dresselhaus, *Phys. Rev. B* **1993**, *47*, 12727-12731.
[57] L. D. Hicks, T. C. Harman, X. Sun, M. S. Dresselhaus, *Phys. Rev. B Condens. Matter.* **2002**, *281*, 450-453.
[58] D. L. Medlin, G. J. Snyder, *Curr. Opin. Colloid Interface Sci.* **2009**, *14*, 226-235.
[59] M. S. Dresselhaus, G. Chen, M. Y. Tang, R. Yang, H. Lee, D. Wang, Z. F. Ren, J-P Fleurial, *Adv. Mater.* **2007**, *19*, 1043-1053.
[60] Y. Lan, A. J. Minnich, G. Chen, Z. Ren, *Adv. Mater* **2010**, *20*, 357-376.
[61] M. Scheele, N. Oeschler, K. Meier, A. Kornowski, C. Klinke, H. Weller, *Adv. Funct. Mater.* **2009**, *19*, 3476-3483.
[62] B. Poudel, Q. Hao, Y. Ma, Y. Lan, A. Minnich, B. Yu, X. Yan, D. Wang, A. Muto, D. Vashaee, *Science* **2008**, *320*, 634-638.
[63] W. Xie, X. Tang, Y. Yan, Q. Zhang, T. M. Tritt, *J. Appl. Phys.* **2009**, *105*, 113713.
[64] H. Y. Lv, H. J. Liu, L. Pan, Y. W. Wen, X. J. Tan, J. Shi, X. F. Tang, *Appl. Phys. Lett.* **2010**, *96*, 710-712.
[65] Joseph P. Heremans, C. M. Thrush, D. T. Morelli, *Phys. Rev. B* **2004**, *70*, 2516-2528.
[66] Joseph. P. Heremans, M. T. Christopher, T. M. Donald, *J. Appl. Phys.* **2005**, *98*, 063703.
[67] J. Heremans, *Springer Berlin Heidelberg* **2007**, 345-374.
[68] S. N. Girard, J. He, X. Zhou, D. Shoemaker, C. M. Jaworski, C. Uher, V. P. Dravid, J. P. Heremans, M. G. Kanatzidis, *J. Am. Chem. Soc.* **2011**, *133,* 16588-16597.
[69] Y. Pei, X. Shi, A. Lalonde, H. Wang, L. Chen, G. J. Snyder, *Nature* **2011,** 473, 66-69.
[70] H. Wang, J-F. Li, M. Zou, T. Sui, *Appl. Phys. Lett.* **2008**, *93*, 202106.
[71] B. Du, H. Li, J. Xu, X. Tang, C. Uher, *J. Solid State Chem.* **2011**, *184*, 109-114.
[72] K. F. Hsu, S. Loo, F. Guo, W. Chen, J. S. Dyck, C. Uher, T. Hogan, E. K. Polychroniadis, M. G. Kanatzidis, *Science* **2004**, *303*, 818-821.
[73] P. F. Poudeu, J. D'Angelo, A. D. Downey, J. L. Short, T. P. Hogan, M. G. Kanatzidis, *Angew. Chem., Int. Ed.* **2006**, *45*, 3835-3829.

[74] L. D. Hicks, M. S. Dresselhaus, *Phys. Rev. B* **1993**, 47,12727-12731.
[75] R. Venkatasubramanian, T. Colpitts, E. Watko, M. Lamvik, N. El-Masry, *J. Cryst. Growth* **1997**, *170*, 817-821.
[76] R. Venkatasubramanian, E. Siivola, T. Colpitts, B. O'Quinn, *Nature* **2001**, *413*, 597-602.
[77] H. Beyer, J. Nurnus, H. Böttner, A. Lambrecht, E. Wagner, G. Bauer, *Phys. E* **2002**, *13*, 965-968.
[78] S. M. Lee, D. G. Cahill, R. Venkatasubramanian, *Appl. Phys. Lett.* **1997**, *70*, 2957-2959.
[79] T. Borca-Tasciuc, W. Liu, J. Liu, T. Zeng, D. W. Song, C. D. Moore, G. Chen, K. L. Wang, M. S. Goorsky, L. Radetic, *Superlattices Microstruct.* **2000**, *28*, 199-206.
[80] G. Zeng, A. Shakouri, C. L. Bounty, G. Robinson, E. Croke, P. Abraham, X. Fan, H. Reese, J. E. Bowers, *Electron. Lett.* **1999**, *35*, 2146-2147.
[81] J. Zhou, C. Jin, J. H. Seol, X. Li, *Appl. Phys. Lett.* **2005**, *87*, 133109.
[82] E. J. Menke, M. A. Brown, Q. Li, J. C. Hemminger, R. M. Penner, *Langmuir* **2006**, *22*, 10564-10574.
[83] L. Weber, E. Gmelin, *Appl. Phys. A: Mater. Sci. Process.* **1991**, *53*, 136-140.
[84] C. L. Chen, Y. Y. Chen, S. J. Lin, J. C. Ho, P. C. Lee, C. D. Chen, S. R. Harutyunyan, *J. Phys. Chem. C* **2010**, *114*, 3385-3389.
[85] T. C. Harman, P. J. Taylor, D. L. Spears, M. P. Walsh, *J. Electron. Mater* **2000**, *29*, L1-L2.
[86] O. Bubnova, Z. U. Khan, A. Malti, S. Braun, M. Fahlman, M. Berggren, M. Crispin, *Nat. Mater.* **2011**, *10*, 429-433.
[87] G. H. Kim, L. Shao, K. Zhang, K. P. Pipe, *Nat. Mater.* **2013**, *12*, 719-723.
[88] S. K. Yee, N. E. Coates, A. Majumdar, J. J. Urban, R. A. Segalman, *Phys. Chem. Chem. Phys.* **2013**, *15*, 4024-4032.
[89] Q. Wang, Q. Yao, J. Chang, L. Chen, *J. Mater. Chem.* **2012**, *22*, 17612-17618.
[90] B. Cho, K. S. Park, J. Baek, H. S. Oh, Y. E. K. Lee, M. M. Sung, *Nano Lett.* **2014**, *14,* 3321-3327.
[91] Y. Du, K. F. Cai, S. Chen, P. Cizek, T. Lin, *ACS Appl. Mater. Interfaces* **2014**, *6*, 5735-5743.
[92] H. Ju, J. Kim, *ACS nano* **2016**, *10*, 5730-5739.
[93] H. Ju, J. Kim, *Chem. Eng. J.* **2016**, *297*, 66-73.
[94] J. Choi, J. Y. Lee, S. Lee, C. R. Park, H. Kim, *Adv. Energy Mater.* **2016**, *6*, 1502181.
[95] W. C. Lee, H. S. Li, A. B. Wong, D. D. Zhang, M. L. Lai, Y. Yu, Q. Kong, E. Lin, J. J. Urban, J. C. Grossman, P. D. Yang, *Proc. Nat. Acad. Sci. USA* **2017**, *114*, 8693-8697.
[96] Y. X. Wang, R. X. Lin, P. C. Zhu, Q. H. Zheng, Q. J. Wang, D. Y. Li, J. Zhu, *Nano Lett.* **2018**, *18*, 2772-2779.
[97] K. J. Erickson, F. Leonard, V. Stavila, M. E. Foster, C. D. Spataru, R. E. Jones, B. M. Foley, P. E. Hopkins, M. D. Allendorf, A. A. Talin, *Adv. Mater.* **2015**, *27*, 3453-3459.
[98] A. Weathers, Z. U. Khan, R. Brooke, D. Evans, M. T. Pettes, J. W. Andreasen, X. Crispin, L. Shi, *Adv. Mater.* **2015**, *27*, 2101-2106.
[99] K. Suemori, S. Hoshino, T. Kamata, *Appl. Phys. Lett.* **2013**, *103*, 153902.
[100] H. W. Ju, J. K. Sun, B. J. Cho, *Energy* **2014**, *73*, 506-512.
[101] P. Sheng, Y. Sun, F. Jiao, C. Di, W. Xu, D. Zhu, *Synth. Met.* **2014**, *193*, 1-7.
[102] C. A. Hewitt, D. S. Montgomery, R. L. Barbalace, R. D. Carlson, D. L. Carroll, *J. Appl. Phys.* **2014**, *115*, 184502.
[103] W. Zhou, Q. Fan, Q. Zhang, L. Cai, K. Li, X. Gu, F. Yang, N. Zhang, Y. Wang, H. Liu, *Nat. Commun.* **2017**, *8*, 14886.
[104] A. K. Menon, O. Meek, A. J. Eng, S. K. Yee, *J. Appl. Polym. Sci.* **2016**, 134, 44060.
[105] T. Fukumaru, F. Tsuyohiko, N. Naotoshi, *Sci. Rep.* **2015**, *5*, 7951.
[106] C. Yu, A. Murali, K. Choi, Y. Ryu, *Energy Environ. Sci.* **2012**, *5*, 9481-9486.
[107] R. Tian, C. Wan, Y. Wang, Q. Wei, T. Ishida, A. Yamamoto, A. Tsuruta, W. Shin, S. Li, K. Koumoto, *J. Mater. Chem. A* **2017**, *5*, 564-570.
[108] C. Wan, R. Tian, A. B. Azizi, Y. Huang, Q. Wei, R. Sasai, S. Wasusate, T. Ishida, K. Koumoto, *Nano Energy* **2016**, *30*, 840-845.
[109] Q. Wei, M. Mukaida, K. Kirihara, Y. Naitoh, T. Ishida, *Rsc Adv.* **2014**, *4*, 28802-28806.
[110] K. Suemori, H. Satoshi, K. Toshihide, *Appl. Phys. Lett.* **2013**, *103*, 153902.
[111] N. Toshima, K. Oshima, H. Anno, T. Nishinaka, S. Ichikawa, A. Iwata, Y. Shiraishi, *Adv. Mater.* **2015**, *27*, 2246-2251.
[112] F. Rettig, M. Ralf, *Sens. Actuators, B* **2007**, *123*, 413-419.
[113] W. Shin, M. Matsumiya, N. Izu, N. Murayama, *Sens. Actuators, B* **2003**, *93*, 304-308.
[114] W. Shin, M. Matsumiya, F. Qiu, N. Izu, N. Murayama, *Actuators, B* **2004**, *97*, 344-347.
[115] M. Matsumiya, W. Shin, N. Izu, N. Murayama, *Sens. Actuators, B* **2003**, *93*, 309-315.
[116] W. Shin, K. Imai, N. Izu, N. Murayama, *Jpn. J. Appl. Phys.* **2001**, *40*, L1232-L1234.
[117] H. Sturm, E. Brauns, T. Seemann, V. Zoellmer, W. Lang, *Procedia Eng.* **2010**, *5*, 123-126.

10.1002/anie.201901106

WILEY-VCH

Entry for the Table of Contents

REVIEW

This review aims to overview a new type of multi-functional materials class possessing properties of both organic and inorganic materials, i.e. organic-inorganic thermoelectric materials, have shown their versatile properties and tremendous potential in device and module design with high thermoelectric figures, taking advantage of their unique molecular design and interfacial engineering.

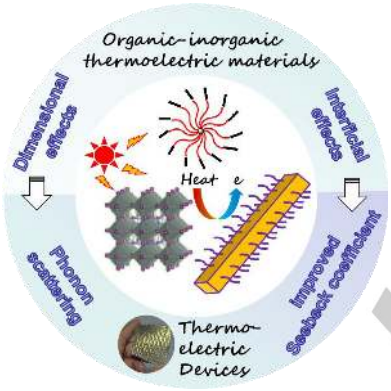

Prof. Dr. Huile Jin, Dr. Jun Li, James Iocozzia, Xin Zeng, Pai-Chun Wei, Chao Yang, Prof. Dr. Nan Li, Dr. Zhaoping Liu, Prof. Dr. Jr Hau He, Prof. Dr. Tiejun Zhu, Prof. Dr. Jichang Wang, Prof. Dr. Zhiqun Lin, Prof. Dr. Shun Wang

Page No. – Page No.

Hybrid Organic-Inorganic Thermoelectric Materials and Devices